

The interactions of fullerene C60 and Benzo(α)pyrene influence their bioavailability and toxicity to zebrafish embryos

This is the peer reviewed version of the following article:

Original:

Della Torre, C., Maggioni, D., Ghilardi, A., Parolini, M., Santo, N., Landi, C., et al. (2018). The interactions of fullerene C60 and Benzo(α)pyrene influence their bioavailability and toxicity to zebrafish embryos. ENVIRONMENTAL POLLUTION, 241, 999-1008 [10.1016/j.envpol.2018.06.042].

Availability:

This version is available <http://hdl.handle.net/11365/1057232> since 2018-08-08T16:35:26Z

Published:

DOI: <http://doi.org/10.1016/j.envpol.2018.06.042>

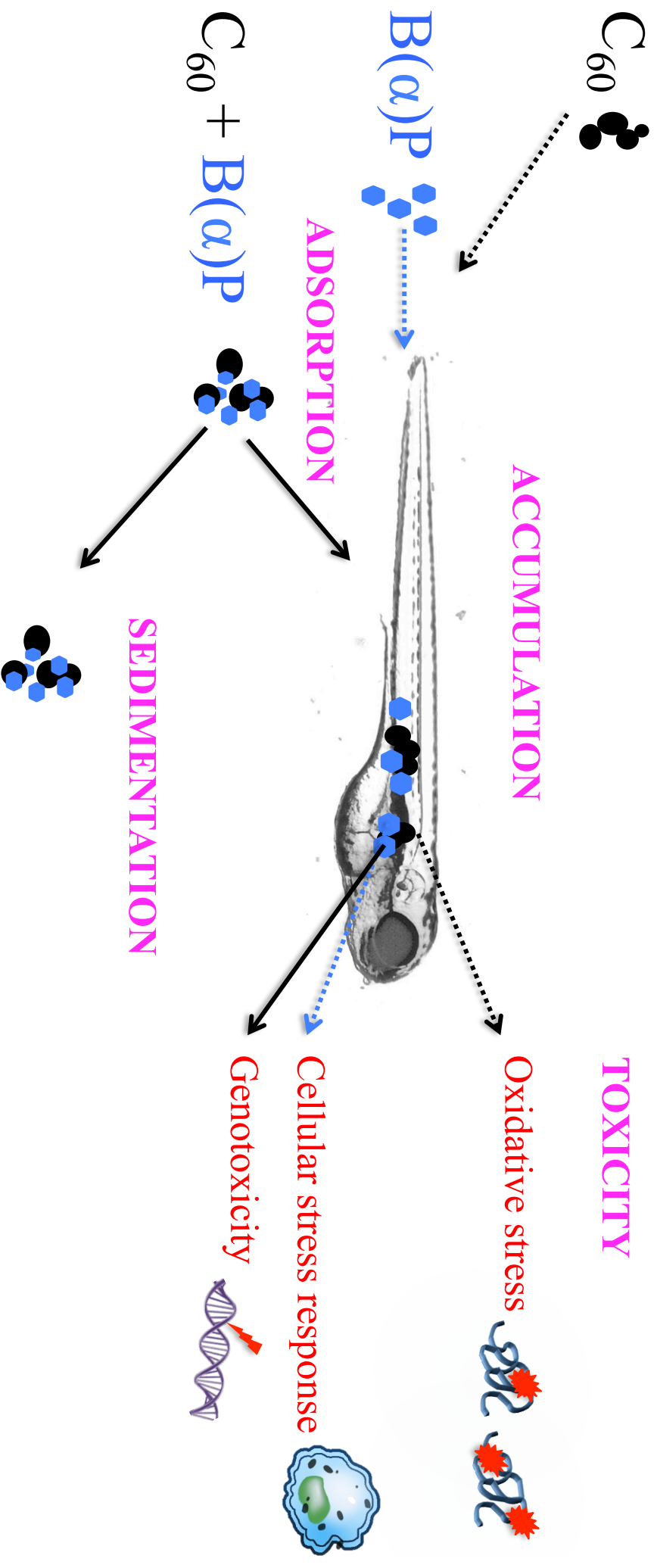
Terms of use:

Open Access

The terms and conditions for the reuse of this version of the manuscript are specified in the publishing policy. Works made available under a Creative Commons license can be used according to the terms and conditions of said license.

For all terms of use and more information see the publisher's website.

(Article begins on next page)



The interactions of Fullerene C₆₀ and Benzo(α)pyrene influence their bioavailability and toxicity to zebrafish embryos

Camilla Della Torre¹, Daniela Maggioni², Anna Ghilardi¹, Marco Parolini³, Nadia Santo¹, Claudia Landi⁴, Laura Madaschi¹, Stefano Magni¹, Stefano Tasselli⁵, Miriam Ascagni¹, Luca Bini⁴, Caterina La Porta³, Luca Del Giacco¹, Andrea Binelli¹

¹Department of Biosciences, University of Milan, Italy

²Department of Chemistry, University of Milan, Italy

³Department of Environmental Science and Policy, University of Milan, Italy

⁴Department of Life Science, University of Siena, Italy

⁵CNR-IRSA (National Research Council-Water Research Institute), Brugherio, Italy

Abstract

This study aimed to assess the toxicological consequences related to the interaction of fullerene nanoparticles (C₆₀) and Benzo(α)pyrene (B(α)P) on zebrafish embryos, which were exposed to C₆₀ and B(α)P alone and to C₆₀ doped with B(α)P. The uptake of pollutants into their tissues and intracellular localization were investigated by immunofluorescence and electron microscopy. A set of biomarkers of genotoxicity and oxidative stress, as well as functional proteomics analysis were applied to assess the toxic effects due to C₆₀ interaction with B(α)P. The carrier role of C₆₀ for B(α)P was observed, however adsorption on C₆₀ did not affect the accumulation and localization of B(α)P in the embryos. Instead, C₆₀ doped with B(α)P resulted more prone to sedimentation and less bioavailable for the embryos compared to C₆₀ alone. As for toxicity, our results suggested that C₆₀ alone elicited oxidative stress in embryos and a down-regulation of proteins involved in energetic metabolism. The C₆₀ + B(α)P induced cellular response mechanisms similar to B(α)P alone, but generating greater cellular damages in the exposed embryos.

Capsule

Once C₆₀ nanoparticles and B(α)P meet in water, they reciprocally affect their bioavailability and, by consequence, their toxicity to organisms.

Keywords: Fullerene nanoparticles; *Danio rerio*; oxidative stress; proteomics; trojan horse effect

1. Introduction

Fullerenes are carbonaceous nanoparticles (NPs) broadly used in several applications including targeted drug delivery systems, lubricants, energy devices, catalysis, surfaces for antiwear applications, cosmetics and sporting goods, due to their outstanding chemico-physical properties (Yadav and Kumar 2008; Mousavi et al., 2017). As a result of the growing production of fullerenes - and especially C₆₀- there is rising concern regarding their presence and impacts on the natural ecosystems. Indeed, fullerenes nanoparticles have been detected in many environmental matrices as atmospheric aerosol (Sanchis et al., 2012) waters (Farrè et al., 2010; Pakarinen et al., 2013; Astefanei et al., 2014), sediments (Sanchis et al., 2015) and soils (Carboni et al., 2016). Therefore, it is extremely important to assess their interactions and toxic effects on wildlife, with particular emphasis on aquatic environments, which act as ultimate sinks for NPs. In fact, the same properties that render fullerenes a unique and innovative material can trigger deleterious effects to natural biocenosis.

The toxicity of C₆₀ has been described in bacteria (Freitas Cordiero et al., 2014), crustaceans (Klaper et al., 2009), bivalves (Canesi et al., 2010; Al-Subiai et al., 2012), chironomids (Waissi et al., 2017) and fishes (Ferreira et al., 2012; Gorrochategui et al., 2017) as well as the potential for trophic transfer (Fortner et al., 2010; Chen et al., 2014). Besides its inherent toxicity, C₆₀ has also exceptional sorption capacity towards hydrophobic chemicals (Hu et al., 2014; Velzeboer et al., 2014) that may significantly affect their bioavailability, bioconcentration and toxicity. Although some studies showed the ability of C₆₀ to sequester diverse contaminants and to reduce their toxicity (Yang et al., 2010; Park et al., 2011), it can conversely act as carrier for organic pollutants enhancing their biological effects on the organisms (Baun et al., 2008; Al-Subiai et al., 2012; Ferreira et al., 2014; Seke et al., 2017; Li et al., 2017). Therefore, the release of C₆₀ into the aquatic environment in the presence of toxic chemicals may pose a further risk for ecosystems, with hardly predictable effects.

56 This study aimed to assess the interactive effects of fullerene NPs (C_{60}) and Benzo(α)pyrene
57 (B(α)P) on zebrafish (*Danio rerio*) embryos. Specifically, we doped C_{60} with B(α)P (C_{60} +B(α)P
58 from now on) and compared the effect on zebrafish embryos exposed to the two contaminants
59 singly administered and to the C_{60} + B(α)P complex. This experimental plan allowed to assess the
60 accumulation and toxicity only of the B(α)P adsorbed on C_{60} without any interference of free
61 hydrocarbon. A thorough evaluation of chemico-physical interactions between the two pollutants
62 has been performed, and the uptake and distribution of C_{60} and B(α)P were shown through
63 advanced microscopy techniques. To evaluate whether C_{60} + B(α)P affects different molecular
64 pathways compared to the two singly administered pollutants, a suite of biomarkers was applied.
65 The activity of proteins involved in the detoxification and antioxidant response, namely glutathione-
66 S-transferase (GST), catalase (CAT) and superoxide dismutase (SOD), was measured, while the
67 oxidative damage was assessed by the measurement of protein carbonylation (PCC). The
68 genotoxicity was assessed by the application of single gel cell electrophoresis (SCGE) assay, DNA
69 diffusion assay and Micronucleus test. Proteomics analysis was also performed to evaluate changes
70 of embryos proteome profile, and suggesting possible mechanisms of action of the pollutants, both
71 alone or in combination.

72

73 **2. Materials and Methods**

74 **2.1 Materials**

75 C_{60} (CAS number: 99685-96-8) and all reagents used for chemical and biomarker analyses were
76 purchased by Sigma-Aldrich (Steinheim, Germany). B(α)P powder (CAS number: 50-32-8) was
77 supplied by Dr. Ehrenstorfer, (Augsburg, Germany).

78

79 **2.2 C_{60} characterization**

80 The bulk C_{60} and C_{60} + B(α)P were observed at Zeiss LEO 912ab Energy Filtering TEM operating
81 at 100 kV, at a magnification of 25-50,000x using a CCD-BM/1 K system.

Dynamic Light Scattering (DLS) was used to measure the hydrodynamic diameter (size distribution) and the charges at the surface (ζ -potential) of water suspended C₆₀ nanoparticles. The measurements were performed on a Malvern Zetasizer Nano ZS instrument (Malvern instruments, UK) equipped with a device for the ζ -potential measurement, employing a solid state He-Ne laser (633 nm) as a light source and recovering the scattered light at an angle of 173° (Series software – version 7.02 – Particular Sciences, UK).

2.3 B(α)P sorption on C₆₀

Two aliquots of C₆₀ (200 mg/L) were suspended in 200 mL of MilliQ water and stirred for 15 days at 20 °C. The first aliquot was doped with 1 mg/L B(α)P dissolved in dimethylsulphoxide (DMSO), while the second portion was not contaminated. The two suspensions were stirred for 5 days at 20 °C in the dark. They were then centrifuged at 3,000 x g for 30 min. The precipitated C₆₀ with B(α)P adsorbed were completely dried in an oven at 40 °C and used for embryos exposures. For measuring the B(α)P fraction remaining solubilized in water, the supernatants were treated with toluene (1:5 v/v, respectively) leaving the mixture under stirring for 90 min at 20 °C in order to extract the free B(α)P solubilized in water by liquid/liquid extraction. The amount of B(α)P in toluene solutions was measured by fluorescence detection, as described in Supplementary Materials. The same technique was used to measure the amount of B(α)P adsorbed on C₆₀ NPs. In this case, the samples were prepared by dissolving 5 mg of dried C₆₀ + B(α)P in 200 mL toluene. A sample containing 5 mg of untreated C₆₀ in 200 mL toluene served as a blank.

2.4 Preparation of C₆₀ suspensions and hydrodynamic behaviour in exposure media

The C₆₀ and C₆₀ + B(α)P were suspended and equilibrated at concentration of 20 mg/L, in zebrafish water (ZFW) for 10 days by stirring in the dark at 20 °C. DLS analysis was performed as described above to determine both hydrodynamic diameters and surface charges (ζ potentials) of each sample.

107 To evaluate the sedimentation process, the UV–vis absorbance spectra of the two suspensions were
108 aquired on an Agilent model 8543 spectrophotometer at room temperature.

109

110 2.5 Zebrafish embryo exposure

111 Adult zebrafish of the AB strain were bred in the fish facility of the Department of Biosciences
112 (University of Milan), to obtain 1-cell stage embryos. Our facility is strictly compliant with the
113 Italian legislation (Legislative Decree No. 116/92) concerning animal welfare, as also certified by
114 the authorization released by the Milan municipality (Art. 10 of Legislative Decree No. 116, dated
115 27.1.1992). Animal procedures were carried out in conformity with the relevant guidelines and
116 regulations.

117 To avoid any physical interference with the uptake of C₆₀, removal of chorion with pronase (0.5
118 mg/mL) was performed at 24 h post-fertilization (hpf), immediately prior to the exposure. Embryos
119 were then exposed to B(α)P (8 µg/L), C₆₀ (20 mg/L) and to C₆₀ + B(α)P in Petri dishes in a total
120 volume of 4 mL. B(α)P concentrations were defined based on the effective B(α)P sorption on C₆₀
121 (20 mg/L) measured by emission spectra (see results). A preliminary range-finding assured that
122 concentrations of C₆₀ and B(α)P were not able to produce mortality or any morphological embryos
123 alteration. Control embryos were exposed to zebrafish water (ZFW) and to vehicle (0.08% DMSO)
124 only. The exposure proceeded until 96 hpf under semistatic conditions, renewing the exposure
125 solutions every 24 h in new vessels. To prevent embryos pigmentation for B(α)P visualization in
126 tissues, ZFW was added with 0.003% 1-phenyl 2-thiourea (PTU). For biochemical analyses and
127 proteomics, embryos were stored at -80 °C until processing. For advanced microscopy and
128 genotoxicity assessment, embryos were immediately processed at the end of the exposure as
129 described below. Experiments were run at least 3 times for each analysis.

130

131 2.6 Electron microscopy

132 A detailed description of ultrastructural analysis procedures is reported in Binelli et al. (2017). Ten
133 embryos from each experimental group were fixed in a mixture containing 4% paraformaldehyde
134 and 2.5% glutaraldehyde in 0.1 M sodium cacodylate buffered solution (pH 7.4). Then the embryos
135 were postfixed in 1% OsO₄, dehydrated in a graded ethanol series and infiltrated in Araldite-Epon.
136 Ultrathin sections of about 70 nm were obtained by Ultracut E microtome (Reichert, Austria).
137 Counterstain of sections was not performed to avoid interference with C₆₀ visualization. Digital
138 images were acquired using a CCD-BM/1K system, and image elaboration was performed using the
139 ESI vision software AnalySIS (Soft Imaging Systems, Muenster, Germany).

140

141 2.7 Immunohistochemistry

142 Details of the procedure are described in Binelli et al. (2017). Briefly, embryos were fixed in
143 paraformaldehyde (4%) and cryo-protected. For immunofluorescence, cryostat sections (10 µm)
144 were incubated with primary antibody anti-polycyclic aromatic hydrocarbons (anti-PAHs 1/100 in
145 PBS, Santa Cruz) and exposed to secondary antibody (Alexa Fluor 488 goat anti-mouse 1:200,
146 Thermo Fisher Scientific). Finally, samples were mounted in PBS/glycerol (1:2 v/v) with DNA-
147 binding dye 40-60-diamidino-2-phenylindole (DAPI). Sections were observed by a confocal
148 microscope Leica SP2 microscope equipped with He/Kr and Ar laser (Leica, Wetzlar, Germany).

149

150 2.8 Accumulation of C₆₀ in zebrafish embryos

151 The quantification of C₆₀ accumulated in zebrafish embryos was performed according to the method
152 described by Waissi et al. (2017), with slight modifications. Embryos were exposed in triplicate to
153 C₆₀ and C₆₀ + B(α)P and to ZFW only (N = 160 for each treatment). After 96 hpf, embryos were
154 collected and washed with MilliQ water, then homogenized in 1 mL of 2% NaCl solution. Toluene
155 (1 mL) was added, the solution vortexed and transferred in an ultrasonic bath for 15 min. After
156 sedimentation, the toluene fraction was collected and C₆₀ absorbance was measured at 335 nm using
157 a Jenway spectrophotometer (Stone, UK). The baseline absorbance detected in controls was

158 subtracted to absorbance of C₆₀ samples. The C₆₀ concentration was determined based on standard
159 curve (0.01-10 µg/mL $r^2 = 0.9997$).

160

161 2.9 Biomarkers analyses

162 A detailed description of biomarkers analysis is reported in Supplementary Materials. The GST,
163 SOD and CAT activities were analysed on homogenates obtained from pools of 60 embryos for
164 each treatment. PCC was evaluated on homogenates obtained from pools of 80 embryos.

165 Genotoxicity was performed on cells dissociated from a pool of 10 zebrafish embryos (three pools
166 per treatment) according to the methods described in Parolini et al. (2017). Briefly, cell viability
167 was assessed by the trypan blue dye exclusion method. The percentage of DNA in the comet tail
168 and the ratio between migration length and comet head diameter (LDR) were used as endpoints of
169 primary genetic damages. The apoptotic and necrotic cell frequency and the frequency of
170 micronuclei (MN%) were measured as fixed genetic damage.

171

172 2.10 Functional proteomics

173 The analysis was performed on pools of 90 embryos for each experimental group. A detailed
174 description of the procedure is reported by Binelli et al. (2017). Briefly, 200 µg of protein for each
175 group were precipitated using a chloroform/methanol/water mixture (4:1:3 v/v). Proteins
176 resuspended in rehydration (denaturing) buffer were loaded in 18 cm pH 3–10 non-linear gradient
177 IPG strips (GE Healthcare, Milan, Italy) and IEF was performed on the Ettan IPGphor II system
178 (GE Healthcare, USA). Protein separation in the second dimension was performed on 12%
179 acrylamide gel in an Ettan DALTsix electrophoretic unit (GE Healthcare, UK). Gels were died by
180 silver stain (ProteoSilver Plus Silver Stain kit; Sigma Aldrich, Milan, Italy), according to producer
181 instructions. Gel images were analyzed by the ImageMaster 2D Platinum software (Amersham
182 Biosciences, USA). Significant protein differences were investigated comparing gels from controls
183 group (ZFW, DMSO) with those from treatment groups. Spots were statistically evaluated in terms

184 of the mean relative volume (vol.%) using Student's t-test for unpaired samples taking $p < 0.05$ as
185 significant threshold. A further criterion for differential regulation was employed such as minimum
186 2-folds change cut-off relative to controls. Significantly modified protein spots were excised from
187 gels, destained, dehydrated with acetonitrile and digested with trypsin (Sigma Aldrich, Milan,
188 Italy). The proteins were identified by MALDI TOF-TOF (matrix-assisted laser
189 desorption/ionization time of flight) mass spectrometry analysis; the Peptide Mass Fingerprinting
190 (PMF) was performed using an Ultraflex III MALDI-TOF/TOF mass spectrometer (Bruker
191 Daltonics, Billerica, MA, United States). Spectra were analyzed by the Flex Analysis software
192 v.3.0. Mascot (Matrix Science Ltd., London, UK, <http://www.matrixscience.com>). On-line-
193 available software was used for PMF search in NCBI nr or Swiss-Prot/TrEMBL databases with
194 taxonomy set for *Danio rerio*.

195

196 2.11 Statistical analysis

197 Biomarker data were investigated through one-way analysis of variance (ANOVA) after checking
198 for normality and homoscedasticity, taking $p < 0.05$ as significance cut-off. The ANOVA was
199 followed by the Duncan's *post-hoc* test to investigate significant differences between exposure
200 groups. The analyses were performed using the STATISTICA 7.0 software package.

201

202 3. Results and Discussion

203 3.1 C₆₀ characterization

204 The bulk C₆₀ consisted mostly of isometric NPs, with mean diameter estimated by TEM
205 micrographs of about 35.6 ± 10.9 nm and few submicrometric aggregates. A similar structure was
206 observed also for C₆₀ + B(α)P (Fig. S1). The DLS analysis of C₆₀ suspension in MilliQ water (1
207 mg/mL) showed the presence of a homogeneous population of NPs aggregates with hydrodynamic
208 radius of 519 ± 169 nm, and polydispersion index (PDI) of 0.39. The stability of the suspension was

209 confirmed by the highly negative surface charge value (-36 ± 1 mV) derived from a ζ -potential
210 measurement.

211 In ZFW, the Z average measured for C_{60} suspension (20 mg/L) was 899 ± 97 nm with PDI of 0.376,
212 indicating the presence of homogeneous population of NPs (trace red in Fig. 1A). On the contrary,
213 the suspension of $C_{60} + B(\alpha)P$ showed the presence of two aggregate populations, centered at $767 \pm$
214 44 nm and 189 ± 13 nm (trace blue in Fig. 1A) showing also the presence of smaller aggregates.
215 Nevertheless, the counts per second of scattered light in this second set of measurements resulted
216 very poor, indicating that a very quick sedimentation phenomenon occurred. Indeed, the suspension
217 just after the DLS measurement pointed out evident sediment at the bottom of the cuvette (Fig. S2).
218 Moreover, UV-Vis analysis highlighted also a significant sedimentation of $C_{60} + B(\alpha)P$ with respect
219 to C_{60} alone, leading to a decrease of concentration of the suspended NPs in ZFW (Fig. 1B). These
220 results suggested that once contaminated with $B(\alpha)P$, C_{60} NPs were more prone to aggregation and
221 to be easily settled out of suspension.

222 Finally, the ζ potential value of C_{60} alone was -23.4 ± 0.2 mV, and a similar value was measured for
223 C_{60} combined with $B(\alpha)P$, equal to -21.6 ± 0.3 mV.

224

225 3.2 $B(\alpha)P$ sorption on C_{60}

226 A small fraction (2.9 %) of the administered $B(\alpha)P$ was recovered in the water phase after 5 days of
227 contamination, while a marked amount of $B(\alpha)P$ (38%) was adsorbed on C_{60} , equal to 378 $\mu\text{g/g}$.
228 Based on these results, the concentration of $B(\alpha)P$ corresponding to suspensions containing 20
229 mg/L of C_{60} was set to 8 $\mu\text{g/L}$. These results confirmed the sorption capacity of C_{60} towards $B(\alpha)P$
230 in the water media as reported for other PAHs (Baun et al., 2008; Hu et al., 2014). Such findings
231 highlighted that C_{60} could alter significantly the fate and transport of $B(\alpha)P$ in the aquatic
232 ecosystems. Moreover our results suggest that as $B(\alpha)P$ is relatively stable and can move in the
233 atmosphere for a long time, it can bind to atmospheric NP such as C_{60} , and be subsequently
234 introduced in the water environment. The high sedimentation rate observed for the complex $C_{60} +$

235 B(α)P strongly suggests that a relevant fraction of the hydrocarbon adsorbed on C₆₀ could reach and
236 accumulate in the sediments.

237

238 3.3 Accumulation of C₆₀

239 The measurement of C₆₀ body burden showed a higher accumulation in embryos exposed to C₆₀
240 alone (16.32 ± 6.45 ng/embryo, corresponding to three-fold increase) than C₆₀ contaminated with
241 B(α)P (3.90 ± 3.39 ng/embryo). Therefore, the observed increase of C₆₀ sedimentation due to B(α)P
242 adsorption reduced the NPs bioavailability and uptake by the embryos. This result highlight that, in
243 natural conditions, the presence of contaminants in water could significantly influence the
244 environmental fate of C₆₀, potentially enhancing its distribution in sediments. According with our
245 result, a previous study on zebrafish embryos showed that the combination of C₆₀ and Hg²⁺
246 increased NPs size and sedimentation, resulting in a lower accumulation of NPs in embryos,
247 compared to the C₆₀ alone (Henry et al., 2013). Similarly, two other studies on nano-TiO₂ in
248 combination with metals have suggested that chemico-physical interactions (e.g. adsorption)
249 between NPs and contaminants can significantly alter their accumulation in organisms (Pavagadhi
250 et al., 2014; Fan et al., 2016).

251 TEM observations showed a microvilli-mediated internalization of C₆₀ NPs in enterocytes mediated
252 (Fig. 2A). The adsorption of B(α)P on C₆₀ did not modify this behavior, as also doped NPs entered
253 enterocytes, (Fig. 2B). TEM observations confirmed the ability of C₆₀ to pass through the gill cell
254 membranes and accumulate in the epithelium cells (Fig. 2C).

255 3.4 B(α)P accumulation

256 The B(α)P fluorescence signal was detected in gills (Fig. 3C, D) and in the gastrointestinal tract
257 (Fig. 3F, G) of embryos exposed to the hydrocarbon. A similar pattern was revealed also in C₆₀ +
258 B(α)P exposed embryos, showing that C₆₀ can act as carrier for the adsorbed B(α)P. Confocal
259 observations suggested that the B(α)P adsorbed on C₆₀ enters the organism mostly through the

gastrointestinal tract, where it can be released and transferred to other compartments as described for different carbon nanomaterials (CNMs; Wang et al. 2011; Su et al., 2013; Seke et al., 2017). Nevertheless, the mechanisms determining the release of contaminants from CNMs and distribution in the organism are still barely understood, and might vary depending on the CNM. For instance, in our recent study we showed that the B(α)P sorbed on carbon nanopowder (CNPW) was taken up by zebrafish embryos and it followed the physical contaminant distribution rather than its natural accumulation (Binelli et al., 2017). On the contrary, the immunoistochemistry analysis showed that the adsorption on C₆₀ did not affect the embryo B(α)P distribution. It is known that fullerene structures, as well as other allotropic carbon-based materials like carbon nanotubes (CNT), interact with the aromatic moieties of many different molecules by π - π interactions (Lu et al., 2006). Yet the sorption of aromatic hydrocarbons by C₆₀ has been calculated and compared with the ability of CNTs to absorb these small molecules (Huffer et al., 2017), concluding that the sorption by CNTs is stronger than that by C₆₀ and may be attributable, among others, to the smaller surface area of the fullerene aggregates in water with respect to the ones of other CNMs (Yang et al., 2006). Therefore, the small difference in the biodistribution of B(α)P when administered alone or associated to C₆₀, could be due to a faster equilibrium release from this material with respect to the dissociation from other carbon-based materials in the physiological environment as the gastrointestinal fluids.

277

278 3.5 Effects of C₆₀

No mortality or teratogenic effects have been recorded in zebrafish embryos exposed to contaminants alone or in combination. Concerning the oxidative stress biomarkers, exposure to B(α)P determined a significant inhibition of CAT activity compared to DMSO ($p < 0.0001$), but did not affect SOD activity. A significant increase of SOD ($p = 0.0004$) and CAT ($p = 0.01$) activities was observed in embryos exposed to C₆₀ alone. On the other hand, the activity of the two enzymes was restored to control levels following C₆₀ + B(α)P exposure, resulting significantly lower in respect to C₆₀ alone ($p = 0.0003$ for SOD and $p = 0.0013$ for CAT) (Fig. 4A,B). The measurement

286 of protein carbonylation showed an increase in carbonyl content exclusively in embryos exposed to
 287 C₆₀ alone compared to controls ($p = 0.019$; Fig. 4D).
 288 The increase of SOD and CAT activity confirmed the ability of C₆₀ to induce antioxidant response,
 289 as already pointed out in other studies performed on several aquatic models (Usenko et al., 2008;
 290 Klaper et al., 2009; Ferreira et al., 2012; Waissi et al., 2017; Lv et al., 2017). The oxidative stress
 291 generated by C₆₀ was also confirmed by the increase of protein carbonylation -marker of oxidative
 292 damage- observed in embryos exposed to C₆₀ alone. Indeed, the carbonylation of proteins involved
 293 in various cellular mechanisms has been described, as consequence of the oxidative stress generated
 294 following exposure to NPs (Driessen et al., 2015). On the contrary, there was no evidence of
 295 oxidative damage in co-exposure, and a significant reduction of the activity of antioxidant enzymes
 296 was observed in comparison to the single pollutant. This result is likely related to the lower
 297 accumulation of C₆₀ observed in embryos exposed to the B(α)P doped NPs in respect to C₆₀ alone,
 298 therefore unable to induce a measurable cellular response.
 299 A significant increase of GST activity was observed in embryos exposed to B(α)P ($p = 0.012$) and
 300 C₆₀ ($p = 0.0002$ vs control) administered alone. GST is involved in phase II of
 301 metabolism/detoxification catalyzing the conjugation of glutathione to several environmental
 302 pollutants and oxidative stress by-products (van der Oost et al., 2003). The induction of GST
 303 activity upon exposure to C₆₀ alone confirmed the active role of this enzyme in the cellular response
 304 to the NPs, as observed in previous studies (Usenko et al., 2008; Klaper et al., 2009). On the
 305 contrary, it is intriguing that C₆₀ + B(α)P determined a significant reduction of GST activity with
 306 respect to control ($p = 0.0002$) (Fig. 3C). This result agrees with previous observations concerning
 307 CNPW contaminated with B(α)P (Della Torre et al., 2017). The same effect was also reported in a
 308 study on zebrafish hepatocytes exposed to C₆₀ and B(α)P (Ferreira et al., 2014), suggesting a
 309 specific inhibition of this enzyme, which may be due to a physical interaction with the doped NPs.
 310 However, the results obtained so far do not allow the identification of the mechanism underlying
 311 this inhibition.

312 Concerning genotoxicity, the exposure to B(α)P alone increased significantly the DNA % in the
313 comet tail ($p < 0.0001$) as well as the LDR ($p = 0.033$) in respect to DMSO (Fig. 4F,G), but did not
314 induce cell necrosis and occurrence of MN (Fig. 4H,I). Our results confirmed the genotoxic
315 potential of B(α)P, which triggered the onset of DNA damage; its weak effect is likely related to the
316 short exposure time (72 h), which may have been not sufficient to determine fixed genetic damages,
317 as normally expected after exposure to B(α)P (Parolini et al., 2017).

318 The C₆₀ administered alone did not cause any primary or fixed DNA damage compared to controls.
319 The results highlighted the absence of genotoxic effects by C₆₀ in agreement with previous studies
320 showing the low genotoxic potential of C₆₀ (Jacobsen et al., 2008) and the inability to generate
321 primary damage to biological systems both *in vitro* and *in vivo* (Shinoara et al., 2009; Matsuda et
322 al., 2011; Ema et al., 2012).

323 Conversely, in embryos exposed to C₆₀ + B(α)P, a significantly higher frequency of necrotic cells
324 was found compared to control ($p < 0.0001$) and C₆₀ administered alone ($p = 0.0012$) (Fig. 4H).
325 Exposure to C₆₀ + B(α)P also resulted in the increase of MN occurrence compared to controls ($p =$
326 0.047), even if the MN frequency of this group did not exceed 5 % (Fig. 4I). An extremely low
327 frequency of apoptotic cells was found in all exposure conditions ($<2\%$ data not shown). The results
328 highlighted that the adsorption of B(α)P increased the cellular damage with respect to the C₆₀ alone.
329 Two possible hypotheses could explain this effect: the first one suggests that when the pollutants
330 are administered in co-exposure (C₆₀ + B(α)P) they induce an increase of cell disruption without
331 direct interacting with the DNA. Alternatively, the reduction of GST activity elicited by the two
332 contaminants administered together might reduce the detoxifying capacity of the embryos, thus
333 enhancing the genotoxic effects of B(α)P. In support of the latter hypothesis, a higher cell death and
334 genotoxicity, together with the inhibition of GST activity, were observed upon exposure to CNPW
335 and C₆₀ + B(α)P, in previous studies (Ferreira et al., 2014; Della Torre et al., 2017).

336

337 3.6 Functional proteomics

338 The application of proteomics allowed the identification of molecular events involved in the
 339 responses to pollutants alone and in co-exposure. About 2,000 different spots in each analyzed gel
 340 were visualized: 220 spots were in common between DMSO and B(α)P, 235 between control and
 341 C₆₀, and 173 between control and C₆₀+B(α)P (Fig. S3). A significant variation in terms of volume
 342 percentage for 28, 50 and 21 spots was measured for the three treatments, respectively. The final
 343 cut-off (≥ 2 -folds) revealed 23, 34 and 14 varied spots for the treatments in comparison to controls.
 344 The exposure to B(α)P up-regulated 12 different proteins and down-regulated the remaining 11 with
 345 respect to DMSO (Fig. S4). The C₆₀ administered alone down-regulated 31 different proteins and
 346 overregulated 3 of them (Fig. S4). The co-exposure C₆₀ + B(α)P induced a significant over-
 347 regulation of 13 proteins and down-regulation of 1 protein only (Fig. S4). Mass spectrometry
 348 analysis allowed the identification of 12 changed proteins in embryos exposed to B(α)P, 27 proteins
 349 for C₆₀ exposure and 5 varied proteins for the co-exposure (Tab. 1, S1, S2, S3).
 350 Going deeper, a variation in the amount of vitellogenin cleavage products (Vtg_{1,5,7}) was observed
 351 in all the three exposure groups. Vtgs are glycopospholipoproteins, which constitute the yolk-
 352 proteins precursors in all oviparous species, including Teleosts. Vtgs are synthesized in the liver of
 353 female and incorporated into oocytes where, following a proteolytic cleavage, provide essential
 354 nutrients for the embryos (Byrne et al., 1989). Therefore, Vtgs proteolytic cleavage processes are
 355 fundamental for the proper embryo development and the evaluation of Vtgs profiles, both at gene
 356 and protein level, is considered a useful tool for highlighting toxic effects due to various types of
 357 environmental pollutants (Muncke and Eggen 2006; Gundel et al., 2007; 2012; Hanish et al., 2010;
 358 Ponnodurai et al., 2012; Hao et al., 2013). The C₆₀-induced down-regulation of Vtgs is in line with
 359 the effects on zebrafish embryos following exposure to Quantum Dots (Petushkova et al., 2015) and
 360 on adults of *Daphnia magna* exposed to Ag-NPs (Rainville et al., 2014). In this latter study, a
 361 significant reduction of Vtg-like proteins was observed together with an increase in protein
 362 oxidation. Therefore the down-regulation of Vtgs could be due to the protein oxidation processes as
 363 a consequence of the oxidative stress generated by C₆₀.

364 In addition to nutritional function, Vtgs have a protective role towards different stressors (Sun and
 365 Zhang, 2015). Particularly, the involvement of Vtg1-like proteins in the DNA repair mechanism has
 366 been demonstrated in zebrafish embryos (Lai et al., 2006). Therefore, the over-regulation of Vtg1
 367 observed in embryos exposed to B(α)P and to C₆₀ + B(α)P might suggest the induction of a
 368 protective mechanism involved, for instance, in the genotoxic damage repair processes.

369 Another protein engaged in the lipid metabolism and in metabolic processes is the
 370 ApolipoproteinA-I (Apoa1b), which was modulated in embryos exposed to B(α)P and C₆₀
 371 administered singly, albeit in opposite way. The alteration of Apoa1b due to modification –
 372 oxidation for instance- might trigger cytotoxic and degenerative effects, therefore promoting the
 373 onset of circulatory alterations (Park and Cho, 2011; Filipe et al., 2013). Indeed, a recent study
 374 highlighted that the exposure of zebrafish embryos to particulate matter_{2.5} (PM_{2.5}) could enhance the
 375 occurrence of cardiovascular toxicity through the proteolytic degradation of lipoproteins (Kim et al.,
 376 2015). The down-regulation of Apoa1b suggested a similar mechanism also for C₆₀. Conversely, the
 377 over-regulation of Apoa1b measured in embryos exposed to B(α)P paralleled the increase of Vtg1.
 378 Indeed, Apoab1 in fact also owns anti-inflammatory and antioxidant properties (Filipe et al., 2013),
 379 which could contribute to the protective response of the embryos towards this pollutant.

380 The exposure to both contaminants, administered alone and in combination, affected the beta-
 381 hemoglobin (BE1), a protein assigned to oxygen transport. The modulation of BE1 in fish is usually
 382 related to environmental stress conditions, such as modification of temperature, salinity and
 383 hypoxia (Eissa e Wang, 2016), but also to the exposure to environmental pollutants (Duarte et al.,
 384 2010; Narra 2016). The observed alteration of BE1 content might affect oxygen supply, thereby
 385 compromising the development and survival of the embryos.

386 The exposure to C₆₀ induced the down-regulation of several kinases such as muscle creatine kinase
 387 A (Ckma), creatine kinase M-type isoform X1 (Ckmb) and nucleoside diphosphate kinase B
 388 (Nme2b.2). These proteins are involved in cellular signaling, growth and differentiation, as well as
 389 energetic metabolism (Tanimura et al., 2014). The alteration of kinases levels might induce the

onset of negative effects on embryos. Indeed, the loss of Nme2b.2 induced severe vasculature malformations (Feng et al., 2014) and cardiomyopathy (Hippe et al., 2009) in zebrafish embryos. The exposure to B(α)P determined a down-regulation of Type I cytokeratin enveloping layer (Cyt1). Cytokeratins are structural proteins involved in the formation of intermediate filaments of epithelial cells and in the maintenance of cell integrity and adhesion in tissues, promoting resistance to mechanical stress (Padhi et al., 2006). The down-regulation of several keratins (Krt4, Krt5 e Krt8) has been already observed in zebrafish embryos exposed to B(α)P (20 μ g/L) (Binelli et al., 2017), supporting the hypothesis that this chemical is able to affect the functionality of structural proteins.

Another down-regulated protein in embryos exposed to B(α)P is the Fatty Acid Binding Protein7 (Fabp7), a chaperonine responsible for cellular fatty acid transport (Furuhashi and Hotamisligil, 2013). At the embryonic level, Fabp7 plays a key role in the development of the central nervous system and affects proper development of the visual system (Liu et al., 2004). Therefore, B(α)P might alter the development and function of the nervous system and the visual apparatus through the down-regulation of Fabp7, as previously suggested (He et al., 2012; Binelli et al., 2017).

Overall, proteomic analysis confirmed the different mechanism of action of single contaminants and their combination. Results suggested that the oxidative stress generated by C₆₀ triggers a general reduction of the metabolic activity in the embryos, confirming recent findings of Lv and coauthors (2017), who suggested that the toxicity of C₆₀ in *D. magna* might be correlated with oxidative stress and reduction of energy acquisition. On the contrary, B(α)P alone and adsorbed on C₆₀ up-regulated proteins involved in the homeostatic response to cellular stress.

411

412 **4. Conclusions**

413 The present study showed how the adsorption of B(α)P by C₆₀ altered the hydrodynamic behavior
414 of the NPs, consequently reducing their bioavailability and intake by the embryos. We showed that

415 the B(α)P adsorbed on C₆₀ is bioavailable and accumulated in embryos. The integration of data
416 obtained through biomarkers and functional proteomics suggests that B(α)P alone and C₆₀ + B(α)P
417 affect similar cellular mechanisms, with the latter triggering severer cellular damages.
418 Our results highlight that, in the natural environment complex chemico-physical-biological
419 interactions arise, possibly determining unexpected ecotoxicological consequences for the
420 organisms.

421 **Acknowledgements**

422 This study was financially supported by the “Cariplo Foundation” grant number 2013-0817. We are
423 grateful to Giorgio Binelli for his precious advices on statistical analysis.

425 **Figure Captions**

426 **Figure 1 C₆₀ characterization.** DLS profile of C₆₀ alone and contaminated with B(α)P, in zebrafish
427 water (A). Particle size distribution of 3 measurements of 10 runs is given by numbers. UV-Vis
428 spectra of C₆₀ suspensions (B).

429 **Figure 2. C₆₀ observation in embryos.** TEM images showing C₆₀ indicated by arrows in gut (A) of
430 embryos exposed to C₆₀ and in gut (B) and gills (C) of C₆₀ + B(α)P. n = nucleus, m =
431 mitochondrion, mv = microvilli, l = lumen.

432 **Figure 3. B(α)P accumulation.** Cryostate sections showing the uptake of B(α)P (in red) in gills
433 (C,D,E) and digestive apparatus (F,G,H) of zebrafish embryos. Controls (A-B), B(α)P (C,F), C₆₀ +
434 B(α)P (D-G) and C₆₀ (E,H). DNA (nuclei) is marked in blue (DAPI coloration). SB = swim bladder,
435 L = gut lumen, Y = yolk sac.

436 **Figure 4. Effects on biomarkers.** Effects on the activity (mean \pm SEM) of SOD (A) CAT (B),
437 GST (C); protein carbonylation (D); and genotoxic effects as DNA strand breaks (E), LDRs (F),
438 occurrence of necrotic cells (G) and MN (H) measured in zebrafish embryos (96 hpf) ($n = 3$; pool of

3 independent experiments). Different letters correspond to values significantly different (one-way ANOVA, Duncan's *post-hoc* test, $p < 0.05$).

References

1. Al-Subiai, S.N., Arlt, V.M., Frickers, P.E., Readman, J.W., Stolpe, B., Lead, J.R., Moody, A.J., Jha, A.N., 2012. Merging nano-genotoxicology with eco-genotoxicology: an integrated approach to determine interactive genotoxic and sub-lethal toxic effects of C(60) fullerenes and fluoranthene in marine mussels, *Mytilus sp.*, Mutat. Res. 745, 92-103.
2. Astefanei, A., Núñez, O., Galceran, M.T., 2014. Analysis of C60-fullerene derivatives and pristine fullerenes in environmental samples by ultrahigh performance liquid chromatography-atmospheric pressure photoionization-mass spectrometry, J. Chromatogr. A 1365, 61-71.
3. Baun, A., Sorensen, S.N., Rasmussen, R.F., Hartmann, N.B., Koch, C.B., 2008. Toxicity and bioaccumulation of xenobiotic organic compounds in the presence of aqueous suspensions of aggregates of nano-C-60. Aquat. Toxicol. 86, 379-387.
4. Binelli, A., Del Giacco, L., Santo, N., Bini, L., Magni, S., Parolini, M., Madaschi, L., Ghilardi, A., Maggioni, D., Ascagni, M., Armini, A., Prosperi, L., Landi, C., La Porta, C., Della Torre, C., 2017. Carbon Nanopowder act as a Trojan-horse for Benzo(a)pyrene in *Danio rerio* embryos. Nanotoxicology 11, 371-381.
5. Byrne, B.M., Gruber, M., Gruber, A.B., 1989. The evolution of yolk proteins. Progr. Biophys Mol. Biol. 53, 33-69.
6. Carboni, A., Helmus, R., Parsons, J.R., Kalbitz, K., de Voogt, P., 2016. A method for the determination of fullerenes in soil and sediment matrices using ultra-high performance liquid chromatography coupled with heated electrospray quadrupole time of flight mass spectrometry. J. Chromatogr. A 1433, 123-130.
7. Canesi, L., Fabbri, R., Gallo, G., Vallotto, D., Marcomini, A., Pojana, G., 2010. Biomarkers in *Mytilus galloprovincialis* exposed to suspensions of selected nanoparticles (Nano carbon black, C60 fullerene, Nano-TiO₂, Nano-SiO₂). Aquat. Toxicol. 100, 168-177.

8. Chen, Q., Yin, D., Li, J., Hu, X., 2014. The effects of humic acid on the uptake and depuration of fullerene aqueous suspensions in two aquatic organisms. *Environ. Toxicol. Chem.* 33, 1090-1097.
9. Della Torre, C., Parolini, M., Del Giacco, L., Ghilardi, A., Ascagni, M., Santo, N., Maggioni, D., Magni, S., Madaschi, L., Prosperi, L., La Porta, C., Binelli, A., 2017. Adsorption of B(a)P on Carbon Nanopowder affects accumulation and toxicity on zebrafish (*Danio rerio*) embryos. *Environ. Sci: Nano* 4, 1132-1146.
10. Driessen, M.D., Mues, S., Vennemann, A., Hellack, B., Bannuscher, A., Vimalakanthan, V., Riebeling, C., Ossig, R., Wiemann, M., Schnekenburger, J., Kuhlbusch, T.A.J., Renard, B., Luch, A., Haase, A., 2015. Proteomic analysis of protein carbonylation: a useful tool to unravel nanoparticle toxicity mechanisms. *Part. Fibr. Toxicol.* 12,36.
11. Duarte, R.M., Honda, R.M., Val, A.L., 2010. Acute effects of chemically dispersed crude oil on gill ion regulation, plasma ion levels and haematological parameters in tambaqui (*Colossoma macropomum*). *Aquat. Toxicol.* 97, 134-141.
12. Eissa, N., Wang, H-P., 2016. Transcriptional stress responses to environmental and husbandry stressors in aquaculture species. *Rev. Aquacult.* 8, 61–88.
13. Ema, M., Tanaka, J., Kobayashi, N., Naya, M., Endoh, S., Maru, J., Hosoi, M., Nagai, M., Nakajima, M., Hayashi, M., Nakanishi, J., 2012. Genotoxicity evaluation of fullerene C₆₀ nanoparticles in a comet assay using lung cells of intratracheally instilled rats. *Regulat. Toxicol. Pharmacol.* 62, 419–424.
14. Fan, W., Peng, P., Li, X., Ren, J., Liu, T., Wang, X., 2016. Effect of titanium dioxide nanoparticles on copper toxicity to *Daphnia magna* in water: Role of organic matter. *Water Res.* 105, 129-137.
15. Farre, M., Perez, S., Gajda-Schranz, K., Osorio, V., Kantiani, L., Ginebreda, A., Barceló, D., 2010. First determination of C₆₀ and C₇₀ fullerenes and N- methylfullereopyrrolidine C₆₀ on the suspended material of wastewater effluents by liquid chromatography hybrid quadrupole linear ion trap tandem mass spectrometry. *J. Hydrol.* 383, 44–51. □
16. Ferreira, J.L., Lonne, M.N., França, T.A., Maximilla, N.R., Lugokenski, T.H., Costa, P.G., Fillmann, G., Soares, F.A., de la Torre, F.R., Monserrat, J.M., 2014. Co-exposure of the organic nanomaterial fullerene C₆₀ with benzo[a]pyrene in *Danio rerio* (zebrafish) hepatocytes: evidence of toxicological

- interactions. *Aquat. Toxicol.* 147, 76-83.
17. Feng, Y., Gross, S., Wolf, N.M., Butenschön, V.M., Qiu, Y., Devraj, K., Liebner, S., Kroll, J., Skolnik, E.Y., Hammes, H-P., Wieland, T., 2014. Nucleoside Diphosphate Kinase B Regulates Angiogenesis Through Modulation of Vascular Endothelial Growth Factor Receptor Type 2 and Endothelial Adherens Junction Proteins. *Arterioscler. Thromb. Vasc. Biol.* 34, 2292-2300.
 18. Filipe, P., Morlière, P., Silva, J.N., Mazière, J-C., Patterson, L.K., Freitas, J.P., Santus, R., 2013. Plasma Lipoproteins as Mediators of the Oxidative Stress Induced by UV Light in Human Skin: A Review of Biochemical and Biophysical Studies on Mechanisms of Apolipoprotein Alteration, Lipid Peroxidation, and Associated Skin Cell Responses. *Ox. Med. Cell. Longev.* 285825.
 19. Freitas Cordeiro, L., Marques, B.F., Wilges Kist, L., Bogo, M.R., Lopez, G., Pagano, G., Clemes I., Guerreiro, K., Monserrat, J.M., 2014. Toxicity of fullerene and nanosilver nanomaterials against bacteria associated to the body surface of the estuarine worm *Laeonereis acuta* (Polychaeta, Nereididae). *Mar. Environ. Res.* 99, 52-59.
 20. Furuhashi, M., Hotamisligil, G.S., 2008. Fatty acid-binding proteins: role in metabolic diseases and potential as drug targets. *Nat. Rev.* 7, 489-503.
 21. Gorrochategui, E., Li, J., Fullwood, N.J., Ying, G-G., Tian, M., Cui, L., Shen, H., Lacorte, S., Tauler, R., Martin, F.L., 2017. Diet-sourced carbon-based nanoparticles induce lipid alterations in tissues of zebrafish (*Danio rerio*) with genomic hypermethylation changes in brain. *Mutagenesis* 32, 91–103.
 22. Gündel, U., Benndorf, D., von Bergen, M., Altenburger, R., Küster, E., 2007. Vitellogenin cleavage products as indicators for toxic stress in zebra fish embryos: A proteomic approach. *Proteomics* 7, 4541–4554.
 23. Gündel, U., Kalkhof, S., Zitzkat, D., von Bergen, M., Altenburger, R., Küster, E., 2012. Concentration–response concept in ecotoxicoproteomics: Effects of different phenanthrene concentrations to the zebrafish (*Danio rerio*) embryo proteome. *Ecotoxicol. Environ. Saf.* 76, 11-22.
 24. Hanisch, K., Kuster, E., Altenburger, R., Gundel, U., 2010, Proteomic Signatures of the Zebrafish (*Danio rerio*) Embryo: Sensitivity and Specificity in Toxicity Assessment of Chemicals. *Int. J. Proteom.* 630134.

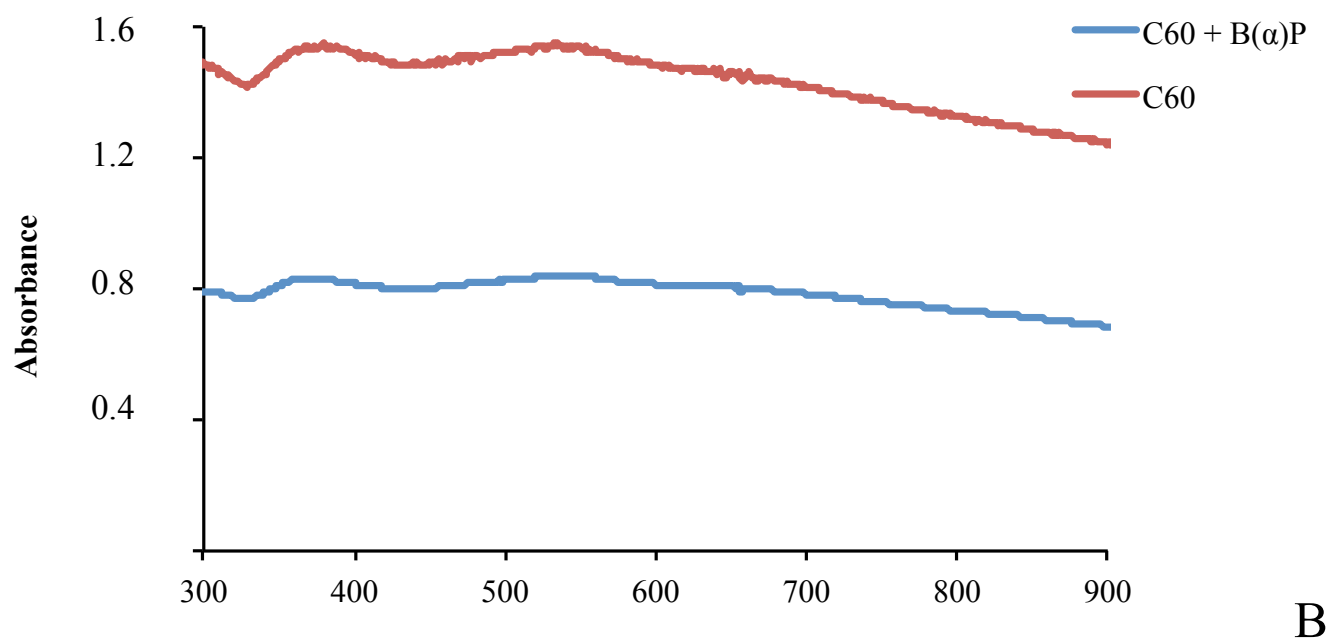
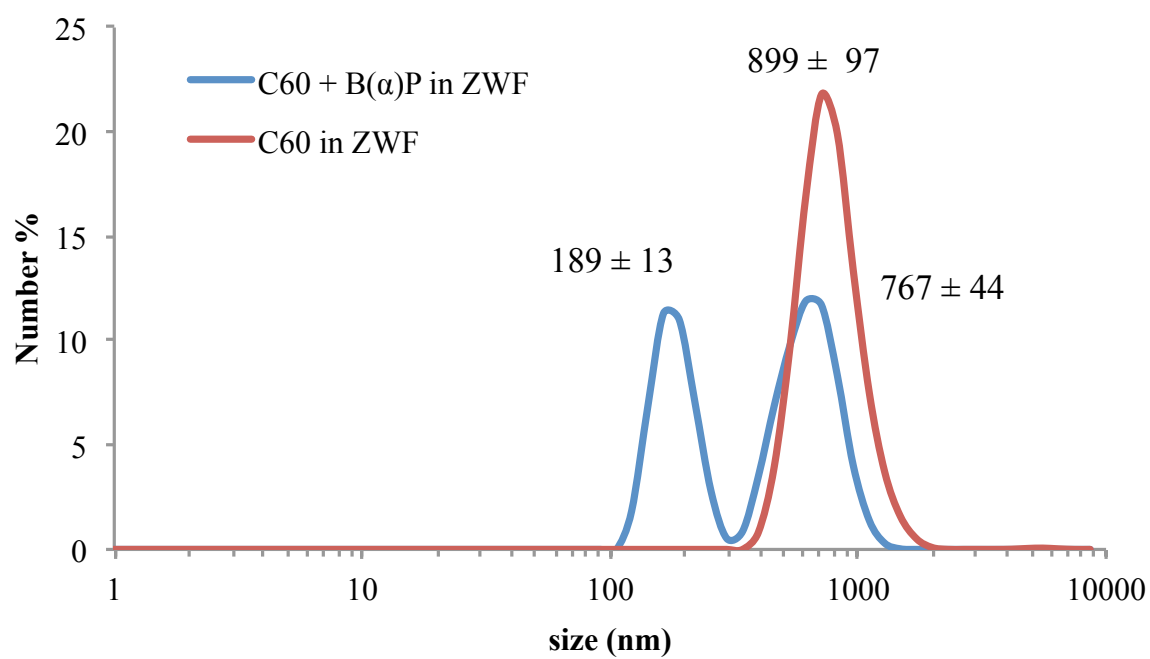
25. Hao, R., Bondesson, W., Singh, A.V., Riu, A., McCollum, C.W., Knudsen, T.B., Gorelick, D.A., Gustafsson, J-A., 2013. Identification of Estrogen Target Genes during Zebrafish Embryonic Development through Transcriptomic Analysis. *PlosOne* 11, e79020.
26. He, C., Wang, C., Zhou, Y., Li, J., Zuo, Z., 2012. Embryonic exposure to benzo(a)pyrene influences neural development and function in rockfish (*Sebastiscus marmoratus*). *Neurotoxicology* 33, 758-762.
27. Henry, T.B., Wileman, S.J., Boran, H., Sutton, P., 2013. Association of Hg²⁺ with aqueous (C₆₀)_n aggregates facilitates increased bioavailability of Hg²⁺ in zebrafish (*Danio rerio*). *Environ. Sci. Technol.* 47, 9997-10004.
28. Hippe, H-J., Wolf, N.M., Abu-Taha, I., Mehringer, R., Just, S., Lutz, S., Niroomand, F., Postel, E.H., Katus, H.A., Rottbauer, W., Wieland, T., 2009. The interaction of nucleoside diphosphate kinase B with G dimers controls heterotrimeric G protein function. *Proceed. Nat. Am. Soc.* 106, 16269-16274.
29. Hu, X., Li, J., Chen, Q., Lin, Z., Yin, D., 2014. Combined effects of aqueous suspensions of fullerene and humic acid on the availability of polycyclic aromatic hydrocarbons: Evaluated with negligible depletion solid-phase microextraction. *Sci. Tot. Environ.* 493, 12-21. □
- 30.** Huffer, T., Sun, H., Kubicki, J.D., Hofmann, T., Kah, M., 2017. Interactions between aromatic hydrocarbons and functionalized C₆₀ fullerenes – insights from experimental data and molecular modelling. *Environ. Sci: Nano* 4, 1045-1052.
31. Jacobsen, N.R., Pojana, G., White, P., Muller, P., Cohn, C.A., Korsholm, K.S., Vogel, U., Marcomini, A., Loft, S., Wallin, H., 2008. Genotoxicity, Cytotoxicity, and Reactive Oxygen Species Induced by Single-Walled Carbon Nanotubes and C₆₀ Fullerenes in the FE1-Muta™ Mouse Lung Epithelial Cells. *Environ. Mol. Mutagen.* 49, 476-487.
32. Kim, J-Y., Lee, E-Y., Inho Choi, I., Kim, J., Cho, K-H., 2015. Effects of the Particulate Matter_{2.5} (PM_{2.5}) on Lipoprotein Metabolism, Uptake and Degradation, and Embryo Toxicity. *Mol. Cells* 38, 1096-1104.
33. Klaper, R., Crago, J., Barr, J., Arndt, D., Setyowati, K., Chen, J., 2009. Toxicity biomarker expression in daphnids exposed to manufactured nanoparticles: Changes in toxicity with functionalization. *Environ. Pollut.* 157, 1152-1156.

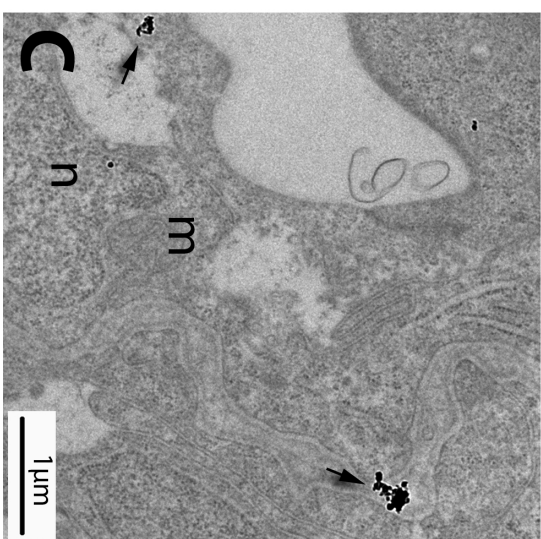
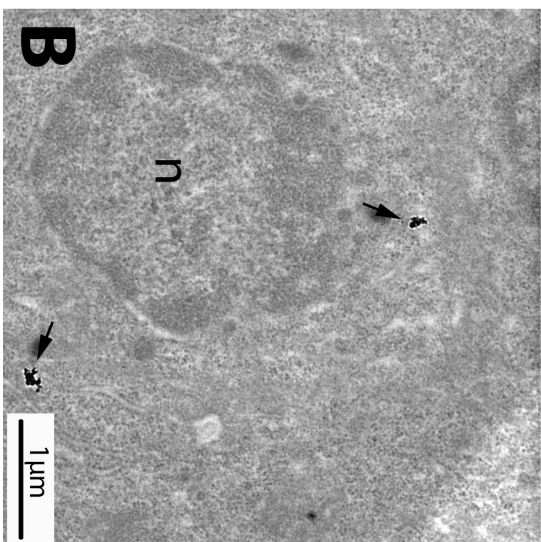
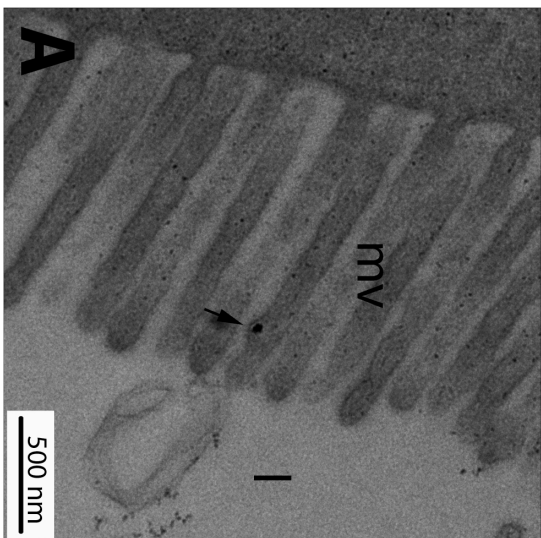
34. Lai, Y-S., Chiue, L-F., Hsu, T., 2006. Low-Molecular-Weight Vitellogenin 1-Like Proteins are Components of a UV-Damaged-DNA Binding Activity Highly Expressed in Zebrafish (*Danio rerio*) Embryos. *J. Exp. Zool.* 305A, 215–224.
35. Li, J., Hu, L-X., Ying, G-G., Martin, F.L, 2017. Co-exposure of C₆₀ fullerene with benzo[a]pyrene results in enhanced biological effects in cells as determined by Fourier-transform infrared spectroscopy. *Environ. Sci: Nano* 4, 1404-1418.
36. Liu, R.Z., Denovan-Wright, E.M., Degrave, A., Thisse, C., Thisse, B., Wright, J.M., 2004. Differential expression of duplicated genes for brain-type fatty acid-binding proteins (fabp7a and fabp7b) during early development of the CNS in zebrafish (*Danio rerio*). *Gen. Express. Patt.* 4, 379–387.
37. Lu, J., Nagase, S., Zhang, X., Wang, D., Ni, M., Maeda, Y., Wakahara, T., Nakahodo, T., Tsuchiya, T., Akasaka, T., Gao, Z., Yu, D., Ye, H., Mei, W.N., Zhou, Y., 2006. Selective Interaction of Large or Charge-Transfer Aromatic Molecules with Metallic Single-Wall Carbon Nanotubes: Critical Role of the Molecular Size and Orientation. *J. Am. Chem. Soc.* 128, 5114–5118.
38. Lv X., Huang, B., Zhu, X., Jiang, Y., Chen, B., Tao, Y., Zhou, J., Cai, Z., 2017. Mechanisms underlying the acute toxicity of fullerene to *Daphnia magna*: Energy acquisition restriction and oxidative stress. *Wat. Res.* 123, 696-703.
39. Matsuda, S., Matsui, S., Shimizu, Y., Matsuda, T., 2011. Genotoxicity of Colloidal Fullerene C60. *Environ. Sci. Technol.* 45, 4133–4138.
40. Mousavi, S.Z., Nafisi, S., Maibach, H.I., 2017. Fullerene nanoparticle in dermatological and cosmetic applications. *Nanomed: Nanotechnol. Biol. Med.* 13, 1071–1087.
41. Muncke, J., Eggen, R.I.L., 2006. Vitellogenin 1 mRNA as an early molecular biomarker for endocrine disruption in developing zebrafish (*Danio rerio*). *Environ. Toxicol. Chem.* 25, 2734–41.
-
42. Narra, M.R., 2016. Single and cartel effect of pesticides on biochemical and haematological status of *Clarias batrachus*: A long-term monitoring. *Chemosphere* 144, 966-974.
43. Padhi, B.K., Akimenko, M-A., Ekker, M., 2006. Independent expansion of the keratin gene family in teleostean fish and mammals: An insight from phylogenetic analysis and radiation hybrid mapping

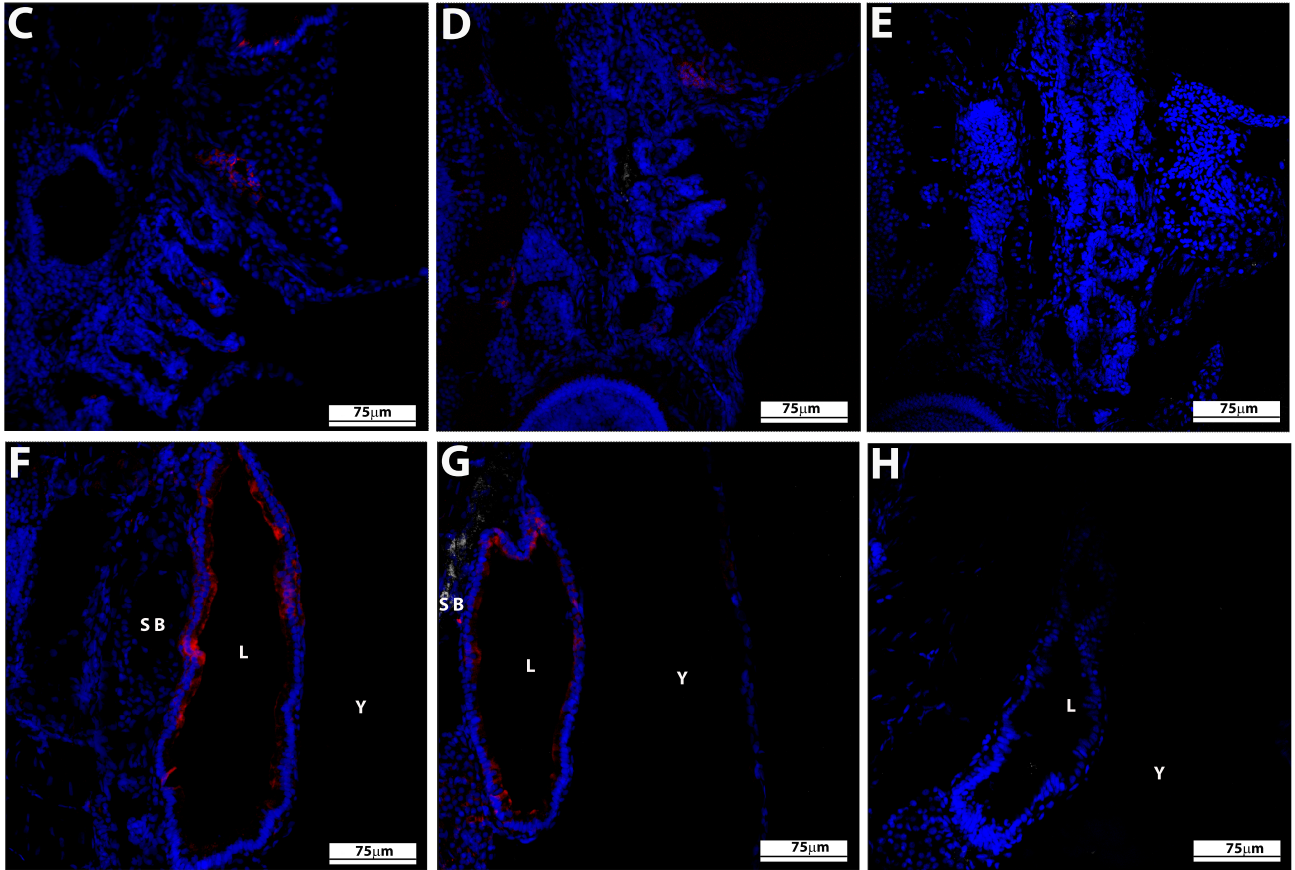
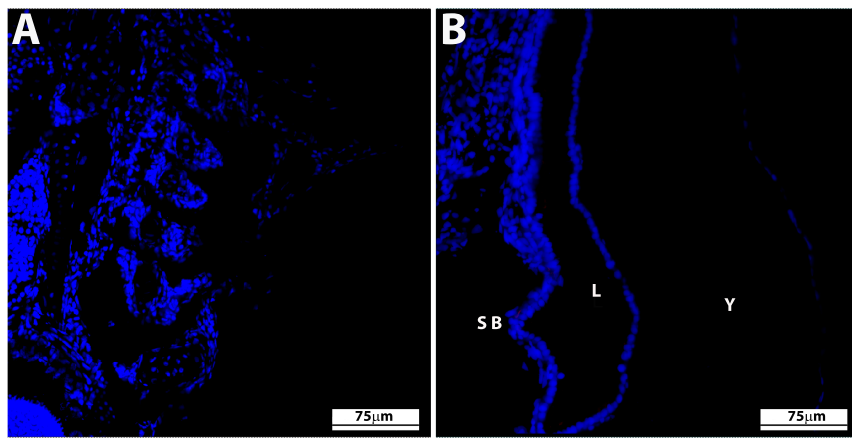
- of keratin genes in zebrafish. *Gene* 368, 37–45.
44. Papaconstantinou, J., 2009. Oxidative modification and aggregation of creatine kinase from aged mouse skeletal muscle. *Aging* 1, 557-572.
 45. Park, K-H., Cho, K-H., 2011. A zebrafish model for the rapid evaluation of pro-oxidative and inflammatory death by lipopolysaccharide, oxidized low-density lipoproteins, and glycated high-density lipoproteins. *Fish Shell. Immunol.* 31, 904-910.
 46. Park, J.W., Henry, T. B., Ard, S., Menn, F. M., Compton, R. N., Sayler, G. S., 2011. The association between nC(60) and 17 alpha- ethinylestradiol (EE2) decreases EE2 bioavailability in zebrafish and alters nanoaggregate characteristics. *Nanotoxicology* 5, 406–416.
 47. Parolini, M., Ghilardi, A., Della Torre, C., Magni, S., Prosperi, L., Calvagno, M., Del Giacco, L., Binelli, A., 2017. Environmental concentrations of cocaine and its main metabolites modulated antioxidant response and caused cyto-genotoxic effects in zebrafish embryo cells. *Environ. Pollut.* 226, 504-514.
 48. Pavagadhi, S., Sathishkumar, M., Balasubramanian, R., 2014. Uptake of Ag and TiO₂ nanoparticles by zebrafish embryos in the presence of other contaminants in the aquatic environment. *Wat. Res.* 55, 280-291.
 49. Petushkova, N.A., Kuznetsova, G.P., Larina, O.V., Kisrieva, Y.S., Samenkova, N.F., Trifonova, O.P., Miroshnichenko, Y.V., Zolotarev, K.V., Karuzina, I.I., Ipatova O.M., Lisitsa A.V., 2015. One-dimensional proteomic profiling of *Danio rerio* embryo vitellogenin to estimate quantum dot toxicity. *Proteom. Sci.* 13, 17.
 50. Ponnudurai RP, Basak T, Ahmad S, Bhardwaj G, Chauhan RK, Singh RA, et al. 2012. Proteomic analysis of zebrafish (*Danio rerio*) embryos exposed to cyclosporine A. *J. Prot.* 75, 1004–17. □
 51. Rainville, L-C., Carolan, D., Varela, A.C., Doyle, H., Sheehan, D., 2014. Proteomic evaluation of citrate-coated silver nanoparticles toxicity in *Daphnia magna*. *Analyst* 139, 1678-1686.
 52. Sanchis, J., Berrojalbiz, N., Caballero, G., Dachs, J., Farre, M., Barcelo, D., 2012. Occurrence of aerosol-bound fullerenes in the mediterranean sea atmosphere. *Environ. Sci. Technol.* 46, 1335–1343. □
 53. Sanchis, J., Oliviera, L.F., Leão, F.B., Farre, M., Barcelo, D., 2015. Liquid chromatography–

- atmospheric pressure photoionization–Orbitrap analysis of fullerene aggregates on surface soils and river sediments from Santa Catarina (Brazil). *Sci. Tot. Environ.* 505, 172–179. □
54. Seke, M., Milica Markelic, M., Morina, A., Jovic, D., Korac, A., Milicic, D., Djordjevic, A., 2017. Synergistic mitotoxicity of chloromethanes and fullerene C₆₀ nanoaggregates in *Daphnia magna* midgut epithelial cells. *Protoplasma* 254, 1607-1616.
 55. Shinohara, N., Matsumoto, K., Endoh, S., Maru, J., Nakanishi, J., 2009. *In vitro* and *in vivo* genotoxicity tests on fullerene C₆₀ nanoparticles. *Toxicol. Lett.* 191, 289-296.
 56. Su, Y., Yan, X.M., Pu, Y.B., Xiao, F., Wang, D.S., Yang, M., 2013. Risks of Single-Walled Carbon Nanotubes Acting as Contaminants- Carriers: Potential Release of Phenanthrene in Japanese Medaka (*Oryzias latipes*). *Environmen. Sci. Technol.* 47, 4704–4710.
 57. Sun, C., Zhang S., 2015. Immune-Relevant and Antioxidant Activities of Vitellogenin and Yolk Proteins in Fish. *Nutrients* 7, 8818–8829.
 58. Tanimura, A., Horiguchi, T., Miyoshi, K., Hagita, H., Noma, T., 2014. Differential Expression of Adenine Nucleotide Converting Enzymes in Mitochondrial Intermembrane Space: A Potential Role of Adenylate Kinase Isozyme 2 in Neutrophil Differentiation. *PlosOne* 9, e89916.
 59. Usenko, C.Y., Harper, S.L., Tanguay, R.L., 2008. Fullerene C₆₀ exposure elicits an oxidative stress response in embryonic zebrafish. *Toxicol. Appl. Pharmacol.* 229, 44–55.
 60. van der Oost, R., Beyer, J., Vermeulen, N.P.E., 2003. Fish bioaccumulation and biomarkers in environmental risk assessment: a review. *Environ. Toxicol. Pharmacol.* 13, 57–149.
 61. van der Ploeg, M.J.C., Baveco, J.M., van der Hout, A., Bakker, R., Rietjens, I.M.C.M., van den Brink, N.W., 2011. Effects of C₆₀ nanoparticle exposure on earthworms (*Lumbricus ruellus*) and implications for population dynamics. *Environmen. Pollut.* 159, 198–203.
 62. Velzeboer, I., Kwadijk, C.J.A.F., Koelmans, A.A., 2014. Strong Sorption of PCBs to Nanoplastics, Microplastics, Carbon Nanotubes, and Fullerenes. *Environ. Sci. Technol.* 48, 4869-4876.
 63. Waissi, G.C., Bold, S., Pakarinen, K., Akkanen, J., Leppänen, M.T., Petersen, E.J., Kukkonen, J.V.K., 2017. *Chironomus riparius* exposure to fullerene-contaminated sediment results in oxidative stress and may impact life cycle parameters. *J. Haz. Mat.* 322, 301-309.
 64. Wang, Z., Zhao, J., Song, L., Mashayekhi, H., Chefetz, B., Xing. B., 2011. Adsorption and

- Desorption of Phenanthrene on Carbon Nanotubes in Simulated Gastrointestinal Fluids. Environ. Sci. Technol. 45, 6018-6024.
65. Yadav, B.C., Kumar, R., 2008. Structure, properties and applications of fullerenes. Int. J. Nanotechnol. Applicat. 2, 15-24.
66. Yang, K., Zhu, L.Z., Xing, B.S., 2006. Adsorption of polycyclic aromatic hydrocarbons by carbon nanomaterials. Environ. Sci. Technol. 40, 1855–1861.
67. Yang, X.Y., Edelman, R.E., Oris, J.T., 2010. Suspended C60 nanoparticles protect against short-term UV and fluoranthene photo-induced toxicity, but cause long-term cellular damage in *Daphnia magna*. Aquat. Toxicol. 100, 202-210.







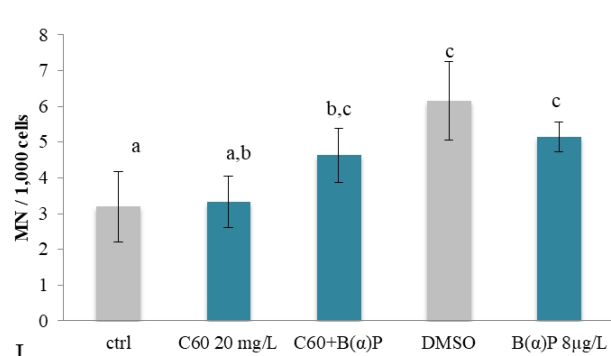
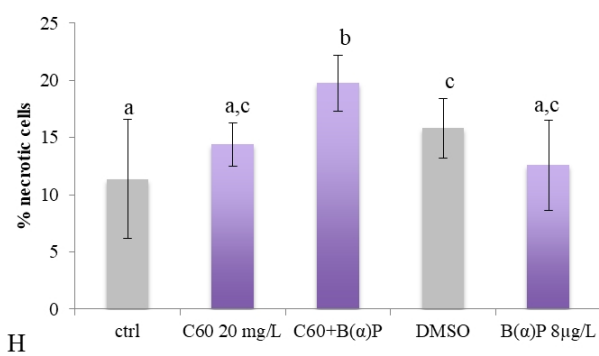
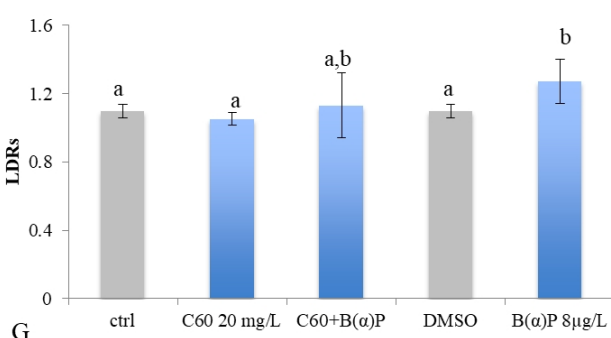
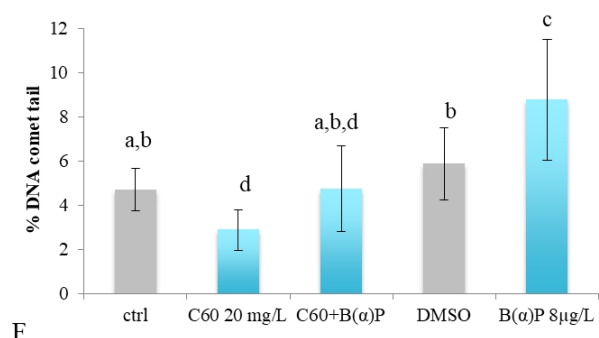
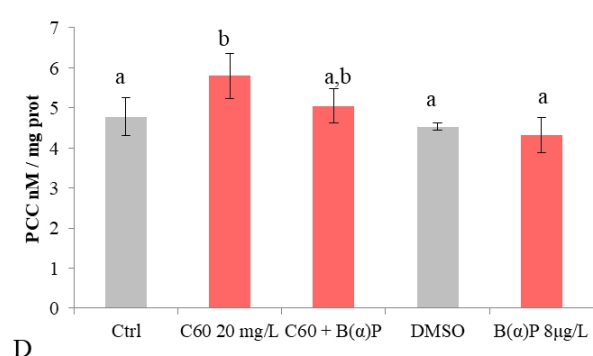
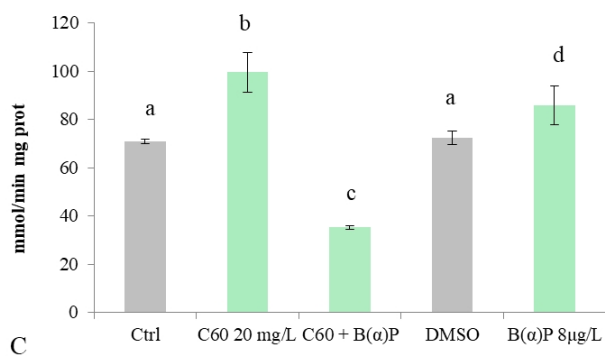
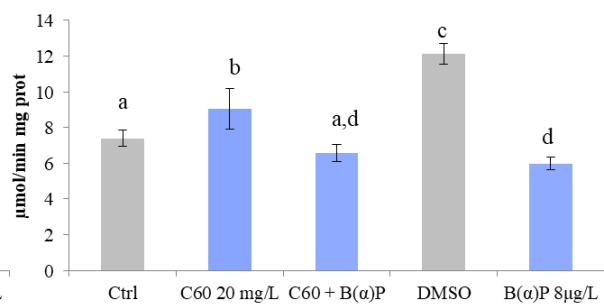
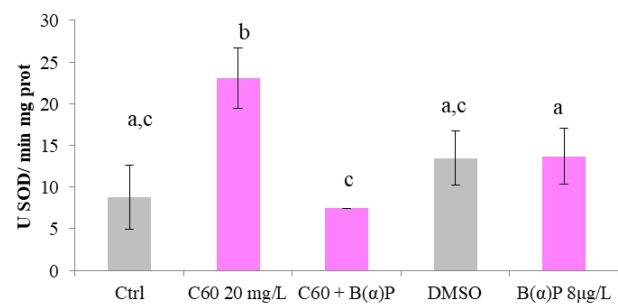


Table1 Proteins modified in zebrafish embryos upon exposure to C₆₀ and B(α)P singly and in combination

<i>Spot</i> ^a	Fold change (↓/↑) ^b	Protein identification	NCBI nr Accession number	Molecular function ^c
B(α)P vs DMSO				
2	2.3↓	Type I cytokeratin, enveloping layer (Cyt1)	AAH65653.1	Structural molecule activity
6	3.2↑	Apolipoprotein A-I precursor (Apoa1b)	NP_001093614.2	Lipid transport
7	3.6↑	Hemoglobin beta embryonic-1.1 (BE1)	NP_932339.1	Oxygen transport
9	2.5↑	Hemoglobin beta embryonic-1.1 (BE1)	NP_932339.1	Oxygen transport
11	2.0↓	Fatty acid binding protein 7, brain, a (Fabp7a)	NP_571680.1	Lipid transport
14	2.9↑	Vitellogenin 1 (Vtg 1)	AAH94995.1	Lipid transport
19	2.8↑	Hemoglobin beta embryonic-1.1 (BE1)	NP_932339.1	Oxygen transport
20	2.5↑	Vitellogenin 1 (Vtg 1)	AAH94995.1	Lipid transport
21	2.5↑	Hemoglobin beta embryonic-1.1 (BE1)	NP_932339.1	Oxygen transport
27	3.6↑	Vitellogenin 1 (Vtg 1)	AAH94995.1	Lipid transport
30	2.0↓	Vitellogenin 5 (Vtg 5)	AAH97081.1	Lipid transport
C₆₀ vs Ctrl				
1	4.0↓	Vitellogenin 1 (Vtg 1)	AAH94995.1	Lipid transport
5	3.5↓	Vitellogenin 1 (Vtg 1)	AAH94995.1	Lipid transport
6	2.9↓	Vitellogenin 1 (Vtg 1)	AAH94995.1	Lipid transport
7	3.0↓	muscle creatine kinase a (Ckma)	NP_571007.2	Kinase activity ATP binding
9	3.4↓	Vitellogenin 1 (Vtg 1)	AAH94995.1	Lipid transport
10	2.1↓	Vitellogenin 1 (Vtg 1)	AAH94995.1	Lipid transport
11	2.0↓	Apolipoprotein A-I precursor (Apoa1b)	NP_001093614.2	Lipid transport
12	3.0↓	Vitellogenin 1 (Vtg 1)	AAK94945.1	Lipid transport
13	2.3↓	Vitellogenin 1 precursor (Vtg 1)	NP_001038362.3	Lipid transport
16	3.7↓	Vitellogenin 1 (Vtg 1)	AAI39514.1	Lipid transport
17	2.7↓	Hemoglobin beta embryonic-1.1 (BE1)	NP_932339.1	Oxygen transport
20	3.2↓	Hemoglobin beta embryonic-1.1 (BE1)	NP_932339.1	Oxygen transport
21	3.2↓	Vitellogenin 1 (Vtg 1)	AAK94945.1	Lipid transport
22	8.1↓	Vitellogenin 1 (Vtg 1)	AAH94995.1	Lipid transport
24	7.2↓	Vitellogenin 7 (Vtg7)	AAW56971.1	Lipid transport
26	2.8↓	muscle-specific creatine kinase (Ckma)	AAK64515.1	Kinase activity ATP binding
27	2.8↓	muscle-specific creatine kinase (Ckma)	AAK64515.1	Kinase activity ATP binding
32	3.1↓	Vitellogenin 1 (Vtg 1)	AAH94995.1	Lipid transport
33	4.9↓	Hemoglobin beta embryonic-1.1 (BE1)	NP_932339.1	Oxygen transport
35	2.6↓	Vitellogenin 1 (Vtg 1)	AAH94995.1	Lipid transport
38	3.0↓	creatine kinase M-type isoform X1 (Ckmb)	XP_005157650.1	Kinase activity ATP binding
43	3.0↓	nucleoside diphosphate kinase B (Nme2b.2)	NP_571002.1	ATP binding
46	2.3↓	Vitellogenin 1 (Vtg 1)	AAK94945.1	Lipid transport
47	3.3↓	Hemoglobin beta embryonic-1.1 (BE1)	NP_932339.1	Oxygen transport
52	2.3↓	Vitellogenin 1 precursor (Vtg 1)	NP_001038362.3	Lipid transport
53	2.7↓	nucleoside diphosphate kinase B (Nme2b.2)	NP_571002.1	ATP binding
54	3.0↓	Vitellogenin 1 (Vtg 1)	AAK94945.1	Lipid transport
C₆₀ + B(α)P vs Ctrl				
1	4.1↑	Vitellogenin 1 (Vtg 1)	AAH94995.1	Lipid transport
5	4.1↑	Vitellogenin 1 (Vtg 1)	AAI39514.1	Lipid transport
7	2.9↑	Vitellogenin 1 (Vtg 1)	AAI39514.1	Lipid transport
8	2.4↑	Hemoglobin beta embryonic-1.1 (BE1)	NP_932339.1	Oxygen transport
12	2.8↑	Vitellogenin 1 (Vtg 1)	AAH94995.1	Lipid transport

^a ID number of spot on 2-DE map;

^b fold change increase (↑) or decrease (↓) in terms of relative spot volume (%V) in comparison with control (ZFW or DMSO);

^c from www.uniprot.org site.

Supporting information

The interactions of Fullerene C₆₀ and Benzo(α)pyrene influence their bioavailability and toxicity to zebrafish embryos

Camilla Della Torre, Daniela Maggioni, Anna Ghilardi, Marco Parolini, Nadia Santo, Claudia Landi, Laura Madaschi, Stefano Magni, Stefano Tasselli, Miriam Ascagni, Luca Bini, Caterina La Porta, Luca Del Giacco, Andrea Binelli

1. Methods

1.1 Fluorescence detection of B(α)P adsorption on C₆₀

Excitation and emission spectra were obtained with an Edinburgh FLS980 spectrofluorometer equipped with a 450 W xenon arc lamp. The spectra were corrected for source intensity (lamp and grating) and emission spectral response (detector and grating) by standard correction curves. The emission spectra of four toluene solutions of B(α)P at different concentrations (0.10, 1.0, 10, 100 mg/L) added with C₆₀ fullerene (25 mg/L) - to take into account possible energy transfer phenomena occurring between B(α)P and C₆₀- were analyzed, and a calibration curve obtained by plotting the intensity maxima of the peaks ($\lambda_{\text{exc}} = 360$ nm, $\lambda_{\text{em}} = 430$ nm). Then, the B(α)P concentration was measured on three independent samples of C₆₀ stock suspension contaminated with B(α)P (1 mg/L) in water, dried, and the aggregates suspended in toluene and analysed for the quantification of the B(α)P adsorbed portion (detection limit ≥ 0.05 mg/L).

1.2 Biomarkers analysis

Embryos were homogenized using a pestle in 100 mM potassium phosphate buffer (KCl 100 mM, EDTA 1 mM, protease inhibitors 1:100 v/v, dithiothreitol 1 mM pH 7.4). The homogenates were centrifuged at 15,000 x g for 10 minutes at 4 °C. The GST activity was measured by adding reduced glutathione (1 mM) in 100 mM phosphate buffer (pH 7.4) and using CDNB (1mM) as substrate. The reaction was monitored for 1 min at 340 nm. The CAT activity was determined by measuring the consumption of H₂O₂ (50 mM) in 100 mM potassium phosphate buffer (pH 7) at 240 nm. The SOD activity was determined by measuring the degree of inhibition of cytochrome c (10 μ M) reduction by the superoxide anion generated by the xanthine oxidase (1.87 mU/mL)/hypoxanthine (50 μ M) reaction at 550 nm. The activity is given as SOD units (1 SOD unit=50% inhibition of the xanthine oxidase reaction). Protein carbonyls were derivatized with 2,4-dinitrophenylhydrazine (DNPH) (10 mM in 2M HCl). Proteins were then precipitated and the pellet washed and resuspended in guanidine hydrochloride (6 M). The absorbance of protein-hydrozone was measured at 370 nm (Mecocci et al., 1999). The total protein content of each sample was measured according to the Bradford (1976) method using bovine serum albumin as standard.

Concerning biomarkers of genotoxicity, first we confirmed that the mean cell viability of dissociated cells from embryos exposed to B(α)P and C₆₀ alone and combined was always higher than the threshold value (70%) suggested for the application of the genotoxicity tests (Kirkland et al., 2007). The alkaline (pH > 13) Single Cell Gel Electrophoresis (SCGE) assay was performed according to the method described in Koshmel et al. (2008). One hundred cells per slide (n = 9; three slides per each pool) were analyzed using the Comet Score[®] image analysis software. The apoptotic cell frequency (%) was assessed analyzing three hundred cells per slide (n=6; two slides per each pool). The frequency of micronuclei (MN‰) was calculated on 400 cells/slide (n=6; two slides per each pool) according to Pavlica et al. (2000).

2. Results

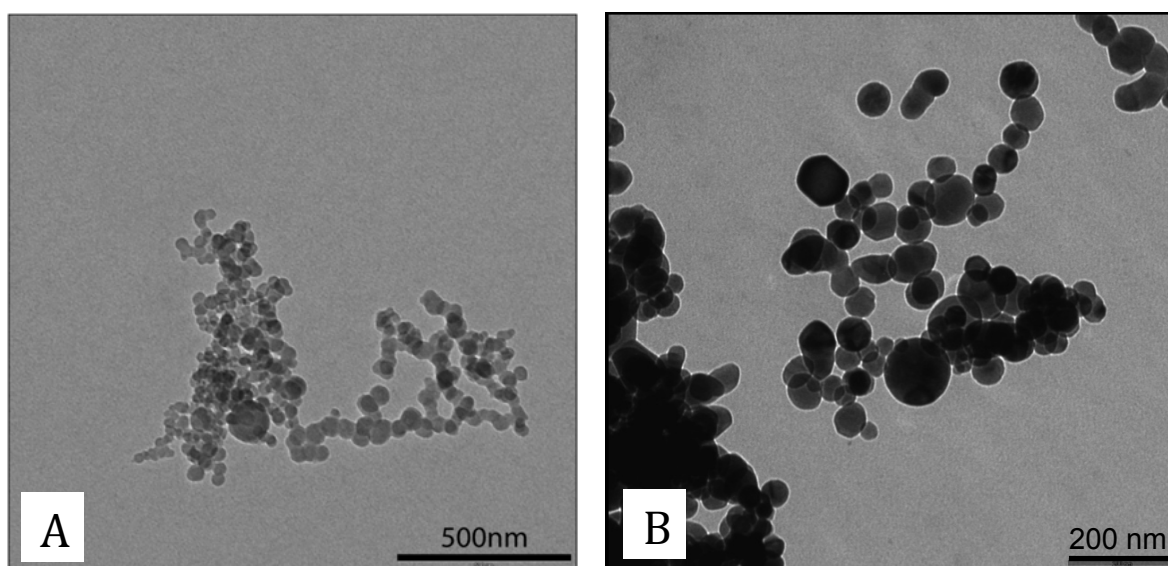


Fig. S1 TEM images of bulk C₆₀ (A) and C₆₀ + B(α)P (B).

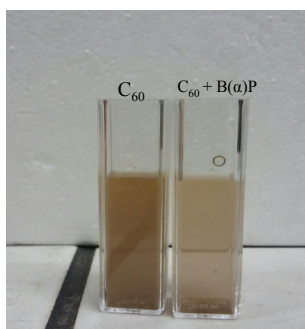


Fig. S2 Sedimentation of suspensions of C₆₀ alone compared to C₆₀ + B(α)P in zebrafish water.

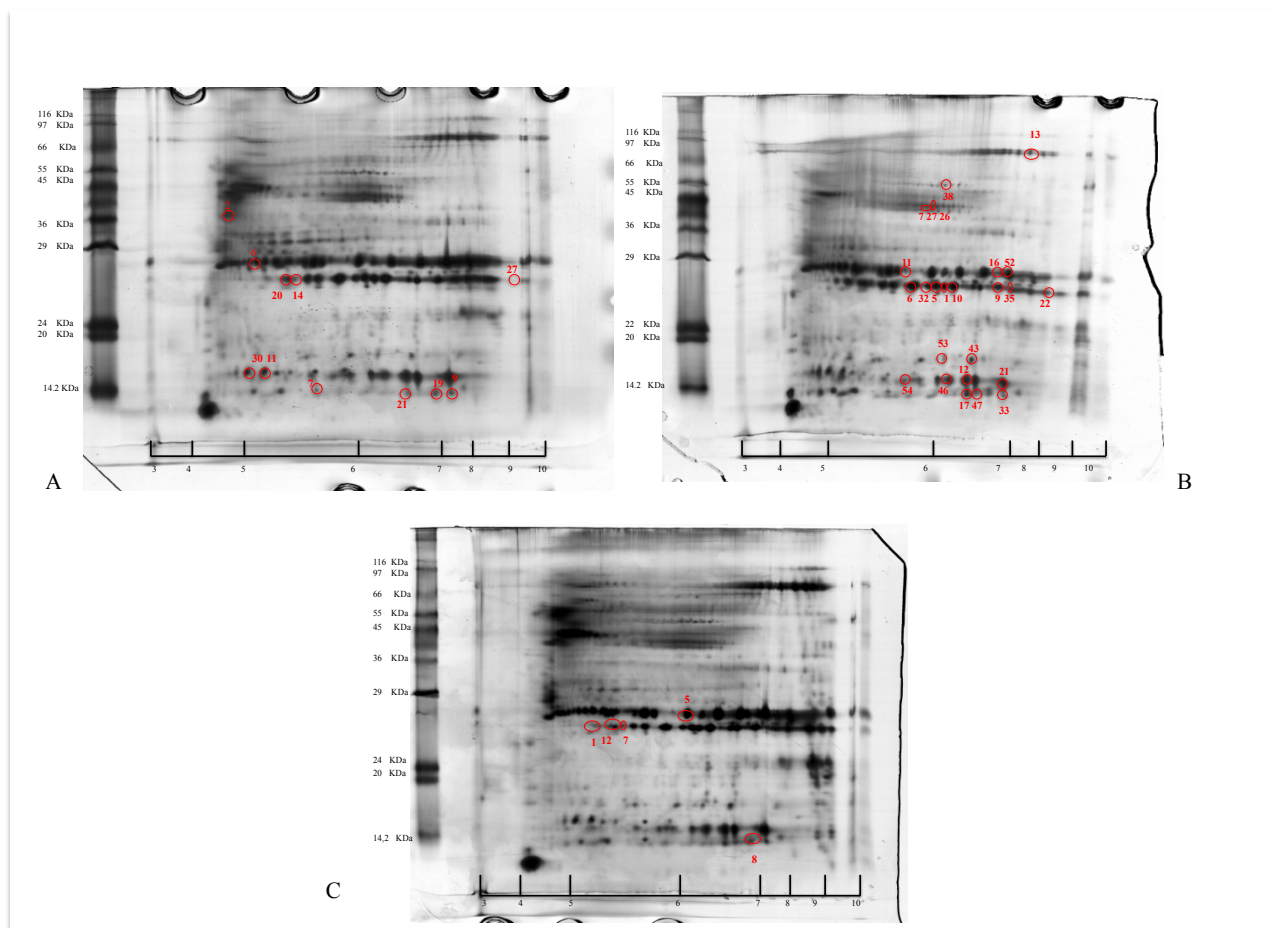


Fig. S3 Representative 2DE gels of zebrafish (96 hpf) exposed to B(α)P and C₆₀ alone and C₆₀ + B(α)P. Red circles highlight proteins identified through mass spectrometry analysis.

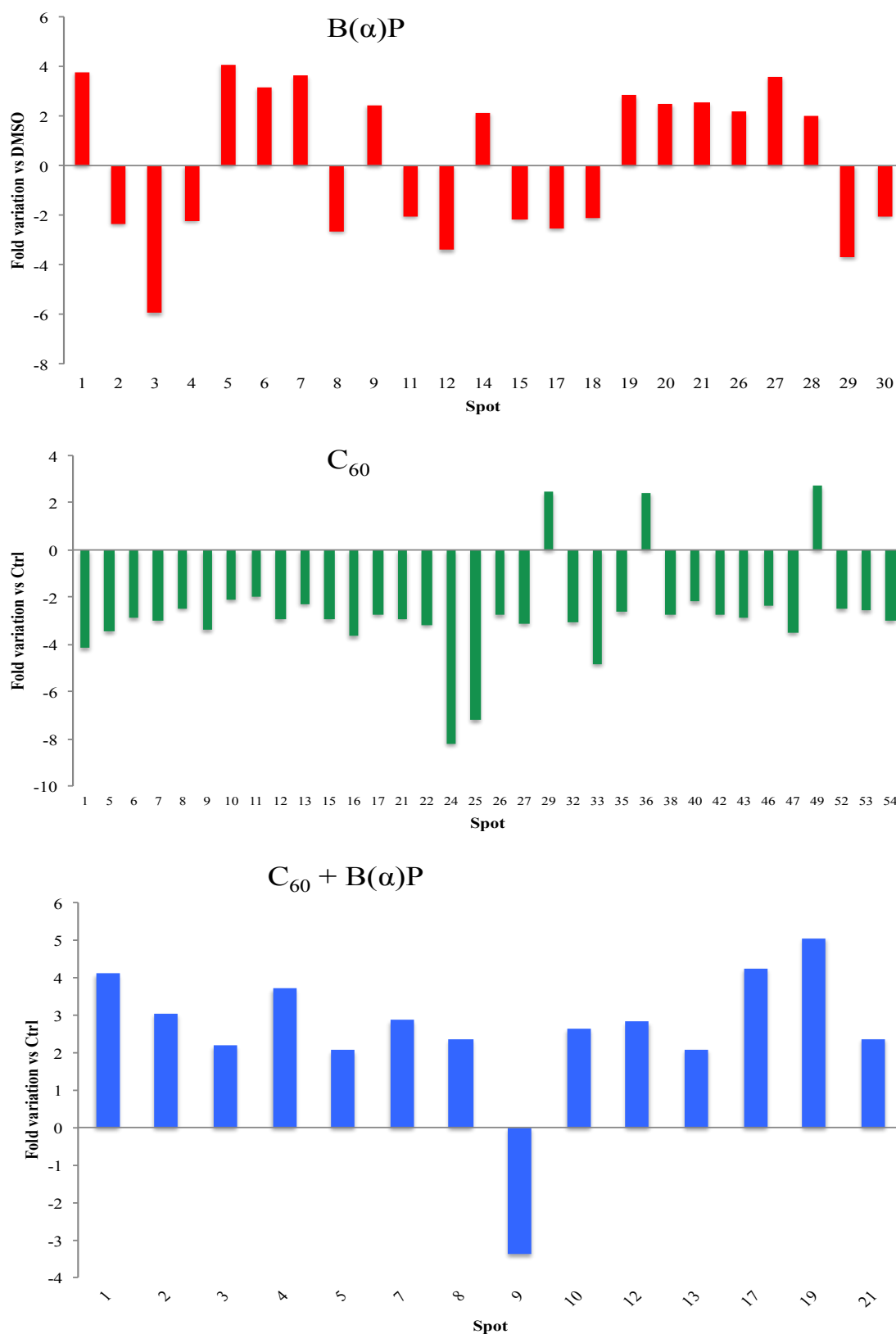


Fig. S4 Protein spots differentially expressed in zebrafish (96 hpf) exposed to B(α)P, C₆₀ and C₆₀ + B(α)P, with respect to controls. The *y-axis* represents the fold change (in terms of relative spot volume, % V) of the protein spots, where a positive value indicates an increase in abundance and a negative value indicates a decrease in abundance.

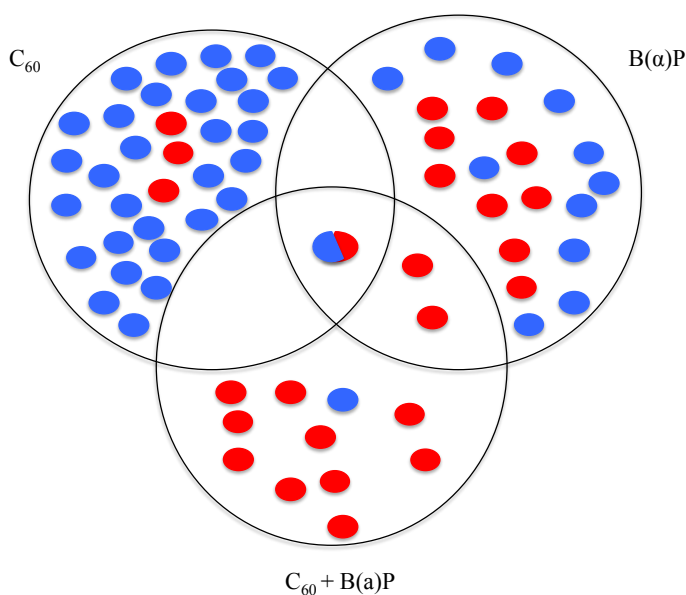


Fig. S5 Venn diagram shows common protein spots between treatments (blue=down-regulation; red=up-regulation).

References

- Bradford, M., 1976. A rapid and sensitive method for the quantitation of microgram quantities of protein utilizing the principle of protein-dye binding. *Analytical Biochemistry* 72, 248-254.
- Kirkland, D.J., Hayashi, D., Jacobson-Kram, M., Kasper, P., MacGregor, J.T., Müller, L., Uno Y. 2007. Summary of major conclusions from the 4th IWGT, San Francisco, 9–10 September. *Mutat. Res.*, 627, 5–9.
- Kosmehl, T., Hallare, A.V., Braunbeck, T., Hollert, H., 2008. DNA damage induced by genotoxicants in zebrafish (*Danio rerio*) embryos after contact exposure to freeze-dried sediment and sediment extracts from Laguna Lake (The Philippines) as measured by the comet assay. *Mutation Research* 650, 1-14.
- Mecocci P., Fano G., Fulle S., MacGarvey U., Shinobu L., Polidori M.C., 1998. Age- dependent increases in oxidative damage to DNA, lipids, and proteins in human skeletal muscle. *Free Radical Biology and Medicine* 26, 303–8.
- Pavlica, M., Klobucar, M., Vetma, G.I.V., Erben, N., Papeš D., 2000. Detection of micronuclei in haemocytes of zebra mussel and ramshorn snail exposed to pentachlorophenol. *Mutation Research* 465, 145–150.

Table S1 Proteins modified in zebrafish embryos (96 hpf) exposed to B(α)P 8 µg/L respect to DMSO

Spot ^a	Fold change (↓/↑) ^b	Protein identification	NCBI ^c Accession number ^c	Molecular function	Theoretical pI/MW (kDa) ^d	Experiment tal pI/MW (kDa) ^e	Mascot search results ^f		
							Sequence coverage (%) ^g	N° of matched peptides ^h	Score ⁱ
2	2.3↓	Type I cytokeratin. enveloping layer (Cyt1) <i>[Danio rerio]</i>	AAH65653.1	Structural molecule activity	46.53/5.13	41.36/4.7	15	6/11	68
6	3.2↑	Apolipoprotein A-1 precursor (Apoalb) <i>[Danio rerio]</i>	NP_001093614.2	Lipid transport	30.18/6.05	30.56/5.1	28	7/11	78
7	3.6↑	Hemoglobin beta embryonic-1.1 (BE1) <i>[Danio rerio]</i>	NP_932339.1	Oxygen transport	16.27/6.89	13.19/5.7	29	4/4	84
9	2.5↑	Hemoglobin beta embryonic-1.1 (BE1) <i>[Danio rerio]</i>	NP_932339.1	Oxygen transport	16.27/6.89	13.19/7.3	29	4/6	73
11	2.0↓	Fatty acid binding protein 7, brain, a (Fabp7a) <i>[Danio rerio]</i>	NP_571680.1	Lipid transport	14.97/5.43	15.09/5.3	40	5/16	70
14	2.9↑	Vitellogenin 1 (Vtg 1) <i>[Danio rerio]</i>	AAH94995.1	Lipid transport	36.58/ 9.23	27.40/5.5	30	7/10	109
19	2.8↑	Hemoglobin beta embryonic-1.1 (BE1) <i>[Danio rerio]</i>	NP_932339.1	Oxygen transport	16.27/6.89	13.19/6.9	29	4/4	84
20	2.5↑	Vitellogenin 1 (Vtg 1) <i>[Danio rerio]</i>	AAH94995.1	Lipid transport	36.58/ 9.23	27.40/5.3	24	7/10	101
21	2.5↑	Hemoglobin beta embryonic-1.1 (BE1) <i>[Danio rerio]</i>	NP_932339.1	Oxygen transport	16.27/6.89	13.19/6.7	29	4/4	84
27	3.6↑	Vitellogenin 1 (Vtg 1) <i>[Danio rerio]</i>	AAH94995.1	Lipid transport	36.58/ 9.23	28.10/9.2	26	7/21	72
30	2.0↓	Vitellogenin 5 (Vtg 5) <i>[Danio rerio]</i>	AAH97081.1	Lipid transport	150.8.77	15.09/5.2	12	12/32	67

^a ID number of spot on 2-DE map;

^b fold change increase (↑) or decrease (↓) in terms of relative spot volume (%V) in comparison with control (DMSO).

^c from www.uniprot.org site;

^d Predicted pI and MW according to protein sequence;

^e Experimentally determined pI and MW;

^f Results obtained by Peptide Mass Fingerprinting analysis;

^g Percentage of sequence coverage of matched peptides in the identified proteins;

^h number of matched peptide/total number of peptide searched;

ⁱ probabilistic score sorted by the software (protein scores greater than 60 were indicated as significant. p<0.05. by the program)

Table S2 Proteins modified in zebrafish embryos (96 hpf) exposed to C₆₀ 20 mg/L respect to Ctrl

<i>Spor^a</i>	Fold change (↓/↑) ^b	Protein identification	NCBI ^c Accession number ^c	Molecular function	Theoretical pI/MW (kDa) ^d	Experimental pI/MW (kDa) ^e	Mascot search results ^f		
							Sequence coverage (%) ^g	N° of matched peptides ^h	Score ⁱ
1	4.0↓	Vitellogenin 1 (Vtg 1) [<i>Danio rerio</i>]	AAH94995.1	Lipid transport	36.58/ 9.23	27.67/6.1	37	13/27	151
5	3.5↓	Vitellogenin 1 (Vtg 1) [<i>Danio rerio</i>]	AAH94995.1	Lipid transport	36.58/ 9.23	27.67/6.0	38	12/22	150
6	2.9↓	Vitellogenin 1 (Vtg 1) [<i>Danio rerio</i>]	AAH94995.1	Lipid transport	36.58/ 9.23	27.67/5.8	48	18/43	167
7	3.0↓	Muscle creatine kinase a (Ckma) [<i>Danio rerio</i>]	NP_571007.2	Kinase activity ATP binding	43/6.32	44.39/6.3	32	11/17	140
9	3.4↓	Vitellogenin 1 (Vtg 1) [<i>Danio rerio</i>]	AAH94995.1	Lipid transport	36.58/ 9.23	27.67/6.8	39	13/29	135
10	2.1↓	Vitellogenin 1 (Vtg 1) [<i>Danio rerio</i>]	AAH94995.1	Lipid transport	36.58/ 9.23	27.67/6.2	41	13/31	144
11	2.0↓	Apolipoprotein A-I precursor (Apoa1b) [<i>Danio rerio</i>]	NP_001093614.2	Lipid transport	30.18/6.05	30.68/5.9	18	5/7	58
12	3.0↓	Vitellogenin 1 (Vtg 1) [<i>Danio rerio</i>]	AAK94945.1	Lipid transport	159/ 8.68	16.25/6.4	11	10/13	99
13	2.3↓	Vitellogenin 1 precursor (Vtg 1) [<i>Danio rerio</i>]	NP_001038362.3	Lipid transport	151/8.74	77.95/8	19	23/35	170
16	3.7↓	Vitellogenin 1 [<i>Danio rerio</i>]	AAI39514.1	Lipid transport	117/ 9.07	30.68/6.9	13	10/23	67

53	2.7↓	nucleoside diphosphate kinase B (Nme2b.2)	NP_571002.1	ATP binding	17.23/6.75	18.56/6.2	37	4/6	71
54	3.0↓	Vitellogenin 1 (Vig 1) [<i>Danio rerio</i>]	AAK94945.1	Lipid transport	150/ 8.68	16.25/5.8	8	8/12	73

^a ID number of spot on 2-DE map;

^b fold change increase (↑) or decrease (↓) in terms of relative spot volume (%V) in comparison with control (ZFW).

^c from www.uniprot.org site;

^d Predicted pI and MW according to protein sequence;

^e Experimentally determined pI and MW;

^f Results obtained by Peptide Mass Fingerprinting analysis;

^g Percentage of sequence coverage of matched peptides in the identified proteins;

^h number of matched peptide/total number of peptide searched;

ⁱ probabilistic score sorted by the software (protein scores greater than 60 were indicated as significant. p<0.05. by the program)

Table S3 Proteins modified in zebrafish embryos (96 hpf) exposed to C₆₀ 20 mg/L + B(α)P 8 μg/L respect to Ctrl

<i>Spot^a</i>	Fold change (↓/↑) ^b	Protein identification	NCBI ^c Accession number ^e	Molecular function	Theoretical pI/MW (kDa) ^d	Experimental pI/MW (kDa) ^e	Mascot search results ^f		
							Sequence coverage (%) ^g	N° of matched peptides ^h	Score ⁱ
1	4.1↑	Vitellogenin 1 (Vig 1) [<i>Danio rerio</i>]	AAH94995.1	Lipid transport	36.58/ 9.23	27.40/5.2	30	9/18	112
5	4.1↑	Vitellogenin 1 (Vig 1) [<i>Danio rerio</i>]	AAI39514.1	Lipid transport	117/ 9.07	30.7/6	10	7/12	93
7	2.9↑	Vitellogenin 1 (Vig 1) [<i>Danio rerio</i>]	AAI39514.1	Lipid transport	117/ 9.07	27.40/5.5	30	7/10	109
8	2.4↑	Hemoglobin beta embryonic-1.1 (BE1) [<i>Danio rerio</i>]	NP_932339.1	Oxygen transport	16.27/6.89	13.19/6.7	29	4/4	84
12	2.8↑	Vitellogenin 1 (Vig 1) [<i>Danio rerio</i>]	AAH94995.1	Lipid transport	36.58/ 9.23	27.40/5.3	24	7/10	101

^a ID number of spot on 2-DE map;

^b fold change increase (↑) or decrease (↓) in terms of relative spot volume (%V) in comparison with control (ZFW).

^c from www.uniprot.org site;

- ^d Predicted pI and MW according to protein sequence;
- ^e Experimentally determined pI and MW;
- ^f Results obtained by Peptide Mass Fingerprinting analysis;
- ^g Percentage of sequence coverage of matched peptides in the identified proteins;
- ^h number of matched peptide/total number of peptide searched;
- ⁱ probabilistic score sorted by the software (protein scores greater than 60 were indicated as significant. $p < 0.05$. by the program)